Trehalose-6-phosphate synthase 8 increases photosynthesis and seed yield in Brassica napus

Article

Accepted Version

Yuan, P., Zhou, G., Yu, M., Hammond, J. P. ORCID: https://orcid.org/0000-0002-6241-3551, Liu, H., Hong, D. ORCID: https://orcid.org/0000-0001-9460-219X, Cai, H. ORCID: https://orcid.org/0000-0002-1430-5126, Ding, G. ORCID: https://orcid.org/0000-0003-3702-5087, Wang, S., Xu, F. ORCID: https://orcid.org/0000-0003-3564-1644, Wang, C. and Shi, L. ORCID: https://orcid.org/0000-0002-5312-8521
(2024) Trehalose-6-phosphate synthase 8 increases photosynthesis and seed yield in Brassica napus. The Plant Journal, 118 (2). pp. 437-456. ISSN 1365-313X doi: 10.1111/tpj.16617 Available at https://centaur.reading.ac.uk/114683/

Trehalose-6-phosphate synthase 8 increases photosynthesis and seed yield in *Brassica napus*

Running Head

BnaC02.TPS8 promotes seed yield in *B. napus*

Pan Yuan[1, 2], Guilong Zhou[3], Mingzhu Yu[1, 2], John P. Hammond[4], Haijiang Liu[1, 2], Dengfeng Hong[1, 5], Hongmei Cai[1, 2], Guangda Ding[1, 2], Sheliang Wang[1, 2], Fangsen Xu[1, 2], Chuang Wang[1, 2], Lei Shi[1, 2, *]

[1]National Key Laboratory of Crop Genetic Improvement, Huazhong Agricultural University, Wuhan, Hubei 430070, China;

[2]Microelement Research Centre, Key Laboratory of Arable Land Conservation (Middle and Lower Reaches of Yangtze River), Ministry of Agriculture and Rural Affairs, Huazhong Agricultural University, Wuhan, Hubei 430070, China;

[3]State Key Laboratory of Hybrid Rice, Institute for Advanced Studies (IAS), Wuhan University, Wuhan, Hubei 430072, China;

[4]School of Agriculture, Policy and Development, University of Reading, Reading RG6 6AR, UK;

[5]National Research Center of Rapeseed Engineering and Technology, National Rapeseed Genetic Improvement Center (Wuhan Branch), Huazhong Agricultural University, Wuhan, Hubei 430070, China

Corresponding author

Lei Shi

Tel: +86 027-87286871

E-mail address: leish@mail.hzau.edu.cn

SUMMARY

Trehalose-6-phosphate (T6P) functions as a vital proxy for assessing carbohydrate status in plants. While class II T6P synthases (TPS) do not exhibit TPS activity, they are believed to play pivotal regulatory roles in trehalose metabolism. However, their precise functions in carbon metabolism and crop yield have remained largely unknown. Here, *BnaC02.TPS8*, a class II TPS gene, is shown to be specifically expressed in mature leaves and the developing pod walls of *Brassica napus*. Over expression of *BnaC02.TPS8* increased photosynthesis and the accumulation of sugars, starch, and biomass compared to wild type. Metabolomic analysis of *BnaC02.TPS8* overexpressing lines and CRISPR/Cas9 mutants indicated that *BnaC02.TPS8* enhanced the partitioning of photoassimilate into starch and sucrose, as opposed to glycolytic intermediates and organic acids, which might be associated with TPS activity. Furthermore, the overexpression of *BnaC02.TPS8* not only increased seed yield but also enhanced seed oil accumulation and improved the oil fatty acid composition in *B. napus* under both high nitrogen (N) and low N conditions in the field. These results highlight the role of class II TPS in impacting photosynthesis and seed yield of *B. napus*, and *BnaC02.TPS8* emerges as a promising target for improving *B. napus* seed yield.

KEYWORDS

Brassica napus, *Trehalose-6-phosphate synthase 8*, net photosynthetic rate, seed yield, seed oil content, carbon metabolism

INTRODUCTION

Trehalose-6-phosphate (T6P) is a key signaling molecule in sucrose availability and carbon (C) metabolism (Schluepmann et al., 2004; Figueroa and Lunn 2016). T6P plays a critical role in regulating sucrose utilization and allocation, and fundamental processes that drive crop growth and yield (Paul et al., 2022). Notably, transgenic maize plants overexpressing rice *OsTPP1* using a floral promoter (MADS6) exhibit reduced T6P concentrations in reproductive tissues, resulting in higher yields under both non-drought and drought conditions (Nuccio et al., 2015). These transgenic maize lines also display enhanced photosynthetic rates and delayed leaf senescence compared to the wild type (Oszvald et al., 2018). Moreover, the application of plant-permeable analogs of T6P directly to plants impacts endogenous T6P concentrations, consequently promoting starch synthesis and potentially improving grain yield in wheat (Griffiths et al., 2016). Recently, it is discovered that the sugar-inducible transcription factor *OsNAC23* can repress *OsTPP1* expression, resulting in elevated T6P concentrations and a 13% to 17% increase in rice yield (Li et al., 2022). This underscores the potential for modifying T6P concentrations to enhance crop yield (Paul et al., 2022).

In plants, T6P is synthesized from UDP-Glc (UDPG) and Glc-6-phosphate (G6P) in a reaction catalyzed by T6P synthase (TPS), followed by the dephosphorylating T6P to trehalose, a reaction catalyzed by T6P phosphatase (TPP) (Cabib and Leloir 1958). In *Arabidopsis*, *TPS* genes are divided into two sub-families, designated class I (*AtTPS1-4*) and class II (*AtTPS5-11*) (Leyman et al., 2001). While AtTPS1 can complement the yeast *tps1*Δ mutant, other class I TPS proteins can complement the *tps1*Δ*tps2*Δ double mutant, indicating that they all have TPS activity (Delorge et al., 2015). Knocking out *AtTPS1* in Arabidopsis results in altered growth and development, including abnormal cell wall morphology and embryo lethality (Eastmond et al., 2002; Gómez et al., 2006). Weak alleles of *AtTPS1*, which are non-embryo-lethal, exhibit delayed flowering and a 40% reduction in T6P concentrations compared to wild type plants (Wahl et al., 2013). In contrast, no class II TPS proteins can complement the yeast *tps1*Δ mutant (Ramon et al., 2009; Delorge et al., 2015). While many of the functions of class II *TPS* genes remain unclear, there is evidence of their diverse roles in growth and development. For instance, *AtTPS5* is involved in thermotolerance and ABA signaling (Suzuki et al., 2008; Tian et al., 2019), while *OsTPS8* enhances salt tolerance by increasing suberin

deposition and the expression of ABA-responsive genes in rice (Vishal et al., 2019). *AtTPS6* has a role in defining the shape of epidermal pavement cells and branching of trichomes (Chary et al., 2008), and *AtTPS11* promotes *Arabidopsis* defense against aphids (Singh et al., 2011). However, there is limited information available on whether class II TPS proteins affect T6P concentrations in plants.

Sucrose-non-fermenting1-related kinase1 (SnRK1) plays a central role in the response to low energy conditions. Evidence suggests that T6P functions as an inhibitor of SnRK1, promoting biosynthetic reactions in young tissues and lateral root formation (Zhang et al., 2009; Lawlor et al., 2014; Morales-Herrera et al., 2023). SnRK1 is involved in the transcriptional regulation of class II TPS genes, such as AtTPS5-AtTPS7 in Arabidopsis, which have been identified as SnRK1 targets (Harthill et al., 2006; Baena-Gonzalez et al., 2007; Cho et al., 2016; Nukarinen et al., 2016), and this regulation is dependent on bZIP11 (Ma et al., 2011). Phosphorylation of these proteins leads to their association with 14-3-3 proteins (Harthill et al., 2006). Recent research indicates that class II TPS can suppress SnRK1 kinase activity and hinder nuclear localization by interacting with the α-catalytic subunit of SnRK1 and co-localized at the endoplasmic reticulum in transient tobacco leaves (Van Leene et al., 2022).

In this study, we identified a class II TPS gene, *BnaC02.TPS8*, primarily expressed in mature leaves and developing pod walls of *B. napus*. Our findings show that *BnaC02.TPS8* mutants exhibit significant reductions in sugars and C accumulation, coupled with reduced net photosynthetic rate, delayed leaf development, lower seed yield, and decreased seed oil accumulation. Furthermore, the overexpression (OE) of *BnaC02.TPS8*, driven by the cauliflower mosaic virus 35S promoter (CaMV-35S), led to increased biomass accumulation at the seedling stage, higher seed yield, and enhanced seed oil content in *B. napus* at maturity. Metabolomic analysis suggested that *BnaC02.TPS8* promoted the partitioning of photoassimilate into starch and sucrose, as opposed to glycolytic intermediates and organic acids, potentially through its TPS activity. These results highlight the important role of *BnaC02.TPS8* in photosynthesis organs (leaves and pod wall), seed yield, and seed oil accumulation in *B. napus.*

RESULTS

Expression pattern and subcellular localization of *BnaC02.TPS8*

The precise functions of class II TPS genes in C metabolism and crop yield remain largely unknown. Our previous work shows that the transcript of *BnaC02.TPS8* was significantly reduced by nitrogen (N) deficiency in whole-transcriptome sequencing of *B. napus* (Yang et al., 2020). To investigate the function of *BnaC02.TPS8* in *B. napus*, the amino acid sequences of *Arabidopsis* AtTPS8 were used for BLAST analysis in the BnTIR database (http://yanglab.hzau.edu.cn/BnTIR; Liu et al., 2021). Five homologous copies of AtTPS8 were identified in *B. napus*. However, gene expression data showed that only two BnTPS8 (BnaC02G0247200ZS, designated as *BnaC02.TPS8*; BnaA02G0186800ZS, designated as *BnaA02.TPS8*) were expressed in multiple tissues, especially in mature leaves and developing pod walls (Figure 1a). Domain analysis showed that BnaC02.TPS8, BnaA02.TPS8 and AtTPS8 contained a conserved Glycosyltransferase family 20 domain (Figure S1). A total of 16 independent transgenic *Arabidopsis* Columbia-0 lines were obtained by utilizing around 2 kb of *BnaC02.TPS8* promoter/5'UTR fused to the GUS reporter gene. Interestingly, strong GUS staining was observed in green stem leaves, but weak GUS expression was detected in senescent rosette leaves (Figure 1b(1),(2)). GUS activity was also detected at the seed-funiculus junction in the green pods but not in yellow pods or seeds (Figure 1b(3),(4); Figure S2). Combining the results of the gene expression pattern of *BnaC02.TPS8* and the tissues-specific expression of GUS driven by the native promoter (Figure 1(a-b)), we conclude that *BnaC02.TPS8* is expressed predominantly in photosynthetic organs: fully expanded mature leaves and developing pod walls.

To analyze the subcellular localization of BnaC02.TPS8, BnaC02.TPS8 was fused with green fluorescent protein (GFP) and transiently expressed in the protoplasts of *Arabidopsis*. Results showed that the green fluorescence signal was co-localized with the cytosol marker (Figure 1c), suggesting that BnaC02.TPS8 is localized in the cytosol.

Generation of *B. napus BnaC02.TPS8* CRISPR mutants and OE lines

To further elucidate the function of *BnaC02.TPS8* in oilseed rape, our initial attempts to develop *BnaC02.TPS8* CRISPR/Cas9 mutants for commercial cultivar 'ZS11' encountered challenges, with the explants exhibited necrosis, and the transformation failed. Consequently, knock-out mutants were generated using CRISPR/Cas9 in the

universal cultivar ‘Westar’. Two distinct mutant alleles (*CR-44* and *CR-153*) were selected (Figure 1d; Table S1). The *CR-44* mutant line had a 33 bp deletion in the first exon of *BnaC02.TPS8*, while the *CR-153* mutant had a 9 bp deletion within the *BnaC02.TPS8* coding region, which resulted in a three amino acid deletion.

BnaC02.TPS8 overexpression (OE) lines were generated from the commercial cultivar ‘ZS11’ driven by the CaMV*35S* promoter. Six T_3 transgenic lines with increased expression of *BnaC02.TPS8* were successfully obtained (Figure 1e). Two independent homozygous lines (OE-33 and OE-38) with higher transcript levels, which resulted in significantly higher biomass accumulation than the WT (Figure S3), were selected for further study.

BnaC02.TPS8 improves biomass production, leaf net photosynthetic rate, and carbon-to-nitrogen ratio

Five-week-old *BnaC02.TPS8* knockout mutants and OE lines were grown under nutrient-sufficient conditions in hydroponics (Figure 2a,b). The shoot and root biomass of *BnaC02.TPS8* mutant lines were significantly less than those of WT ‘Westar’ of seven-week-old plants (Figure 2c,d). In contrast, overexpression of *BnaC02.TPS8* significantly increased shoot and root biomass compared to WT ‘ZS11’ (Figure 2c,d). Additionally, the root-to-shoot ratio was significantly increased in *BnaC02.TPS8*-OE lines compared to WT, but there was no difference between *BnaC02.TPS8* mutants and WT (Figure 2e). The leaf length and width of the fully-expanded 5^{th} leaf in CR-44 and CR-153 were significantly smaller than those in the WT, and the leaf size of OE-33 and OE-38 were significantly higher than those in the WT (Figure 2f,g). Photosynthetic efficiency of hydroponically grown ten-week-old plants showed that mutants had a lower net photosynthetic rate, transpiration rate, and stomatal conductance than those in WT, but the OE plants had a higher net photosynthetic rate and transpiration rate than those in WT (Figure 2h-j). However, there were no differences in stomatal conductance and intercellular CO_2 concentration between OE and WT (Figure 2j,k). In addition, the intercellular CO_2 concentration of mutants was significantly higher than in WT (Figure 2k).

There was no significant difference in total C concentration among *BnaC02.TPS8* mutants, OE-lines and WT plants (Figure 2l). However, the total N concentration was significantly greater in *BnaC02.TPS8* mutants and significantly lower in OE lines

compared to their respective WT plants (Figure 2m). Therefore, compared to the WT, the ratio of total C to total N (C/N ratio) was significantly lower in *BnaC02.TPS8* mutants and was significantly higher in the OE lines (Figure 2n). These suggested that *BnaC02.TPS8* is necessary for maintaining leaf photosynthesis and biomass accumulation and affecting C/N metabolism.

***BnaC02.TPS8* has significant effects on carbohydrate metabolism**

The altered C/N ratio in the various *BnaC02.TPS8* transgenic lines prompted an examination of the sugar composition and starch of these lines. Sugars, starch, sugar-phosphates, and sugar-nucleotide concentrations were quantified in the fully expanded fifth and sixth leaves from the bottom of the seven-week-old plant at the seedling stage. The sucrose and soluble sugar concentrations in the leaves were significantly lower in *BnaC02.TPS8* mutants compared with WT 'Westar' and significantly greater in the OE lines compared with WT 'ZS11' (Figure 3a,b). Notably, the trehalose concentration in leaves of *BnaC02.TPS8* mutants was significantly lower by 26.6%, while that in *BnaC02.TPS8*-OE lines was nearly doubled compared to their WT plants (Figure 3c). The starch concentration in *BnaC02.TPS8* mutants was significantly lower by 26.9%-52.6%, while it was increased by 45.4%-86.1% in OE lines (Figure 3d).

Leaf T6P concentrations were significantly higher in the *BnaC02.TPS8*-OE lines than in the WT. However, there were no obvious changes in the T6P concentrations between *BnaC02.TPS8* mutants and WT (Figure 3e). Among the metabolic intermediates of sucrose synthesis, the concentrations of glucose 6-phosphate (G6P) and sucrose 6-phosphate (S6P) were significantly increased in *BnaC02.TPS8*-OE lines compared to the WT, while S6P was significantly lower in *BnaC02.TPS8* mutants, but G6P was not significantly different between the mutant lines and WT (Figure 3f,g). There were no significant differences in the concentrations of F6P, F1, 6BP, and G1P between *BnaC02.TPS8* transgenic lines and WT (Figure S3). Compared to WT, the concentration of ADPG was significantly lower in CR-44 and CR-153, and was significantly higher in OE lines (Figure 3h). However, the concentration of UDPG was not significantly different in *BnaC02.TPS8* transgenic lines compared to their WTs (Figure 3i).

***BnaC02.TPS8* has significant effects on intermediates of glycolysis and tricarboxylic acid (TCA) cycle**

Compared to WT, the concentrations of 3PGA (3-phosphoglycerate) and PEP

(phosphoenolpyruvate) were significantly lower in *BnaC02.TPS8* mutants and significantly higher in OE lines (Figure 4a,b). In addition, the concentration of pyruvate increased in the mutants but decreased in the OE lines (Figure 4c). Mutation or overexpression of *BnaC02.TPS8* had a significant effect on PEP, and the ratio of PEP to pyruvate was significantly lower in the mutants and higher in OE lines compared with their WTs (Figure 4d). The concentrations of shikimate were significantly higher in *BnaC02.TPS8* mutants, but significantly lower in *BnaC02.TPS8*-OE lines compared to their WTs (Figure 4e).

Significantly higher concentrations of tricarboxylic acid (TCA) pathway intermediates were observed in *BnaC02.TPS8* mutants compared to their WT. Concentrations of citrate, aconitate, isocitrate, 2-OG, and succinate were significantly higher in *BnaC02.TPS8*-OE lines, and were significantly decreased in *BnaC02.TPS8* mutants compared to their respective WT plants (Figure 4f-j). The concentrations of fumarate and malate were increased by 25% and 16% in *BnaC02.TPS8* mutants compared to WT, respectively (Figure 4k,l). The concentration of fumarate was lower in OE-38 than that in WT (Figure 4k). However, there was no significant difference in the concentration of malate between OE lines and WT (Figure 4l). These comparisons suggested that there was a significant increase in the net C assimilation rate in the *BnaC02.TPS8*-OE plants but lower amounts of C within the TCA pathway intermediates, and these were largely offset by increases in sucrose and starch.

BnaC02.TPS8 affects sugar and starch-related enzyme activity and gene expression

The pivotal enzyme in sucrose synthesis is sucrose phosphate synthase (SPS), facilitating the conversion of UDP-glucose and fructose 6-phosphate into sucrose 6-phosphate. Sucrose catabolism involves two primary enzymes: invertase (INV), responsible for breaking down sucrose into glucose and fructose, and sucrose synthase (Susy), which catalyzes the reversible cleavage of sucrose into fructose and either uridine diphosphate glucose or adenosine diphosphate glucose (Ruan 2014). In the leaves, the SPS, soluble acid INV, neutral INV, and Susy activity were significantly lower in *BnaC02.TPS8* mutants but significantly higher in *BnaC02.TPS8*-OE lines compared to their respective WT plants (Figure 5a-d). Pyruvate kinase (PK), a key enzyme in glycolytic pathway, showed significantly higher activity in *BnaC02.TPS8*

mutants but lower activity in *BnaC02.TPS8*-OE lines compared to their WT plants (Figure 5e).

Adenosine diphosphate-glucose pyrophosphorylase (AGPase), the limiting enzyme in starch synthesis exhibited approximately 19.2% lower activity in *BnaC02.TPS8* mutants but 21.5% higher activity in *BnaC02.TPS8*-OE lines compared to their WT plants (Figure 5f). Additionally, compared to WT, total trehalose-6-phosphate synthase (TPS) activity was significantly lower in *BnaC02.TPS8* mutants and significantly higher in *BnaC02.TPS8*-OE lines (Figure 5g). These results indicate that *BnaC02.TPS8* modulates multiple metabolic pathways directly or indirectly, including sucrose, starch, and trehalose metabolism in the leaves of *B. napus*.

To further study the functions of *BnaC02.TPS8* in above mentioned process, we measured the expression of key genes involved in starch synthesis (*GBSS1*, *SBE2.1*, and *SBE2.2*), starch catabolism (*GWD3/PWD*, *BAM1*, and *BAM3*), sugar metabolites transport (*PPT*, *GLT1*, and *SUC2*) and nitrogen metabolism (*NRT1.1*, *NRT1.5*, and *GLN1*) in *BnaC02.TPS8* mutants and OE lines (Figure 6). Genes encoding enzymes of starch biosynthesis and sugar metabolite transport in the leaves showed decreased expression in *BnaC02.TPS8* mutants and increased expression in the *BnaC02.TPS8*-OE lines compared with their WT (Figure 6 a-c, g-i). However, compared with the WT, the expression of genes involved in starch catabolism in leaves was significantly decreased in the *BnaC02.TPS8*-OE plants and only the expression of GWD3/PWD increased significantly in the *BnaC02.TPS8* mutants (Figure 6d-f). Importantly, the expression of genes involved in N metabolism was significantly increased in the roots of *BnaC02.TPS8* mutants, while they were significantly repressed in *BnaC02.TPS8*-OE lines compared to WT plants (Figure 6j-l). The observed expression profiles suggest disruption of *BnaC02.TPS8* alters starch turnover and N metabolism in *B. napus*.

BnaC02.TPS8 is associated with seed yield-related traits

To determine whether *BnaC02.TPS8* controls agronomic traits of *B. napus*, field trials were used to investigate the yield-related traits of *BnaC02.TPS8* mutants and OE lines under high and low N conditions for three years (Figure 7; Table 1). The plant height of *B. napus* was reduced by mutation of *BnaC02.TPS8* under low N conditions, and increased by overexpression of *BnaC02.TPS8* under both high and low N conditions (Figure 7a-e). The seed yield per square meter decreased by 20.3%-29.2% in

BnaC02.TPS8 mutants than in WT at high N and reduced by 42.3%-62.4 at low N (Figure 7f). In contrast, the seed yield per square meter was 26.8%-45% greater in the *BnaC02.TPS8*-OE lines compared with WT 'ZS11' at high N and 38.6-70.1% greater at low N (Figure 7f). The increase of yield of *BnaC02.TPS8*-OE lines was achieved by increasing the pod number per plant and the seed number per pod (Table 1). In contrast, the 1000-seed weight and harvest index were similar in *BnaC02.TPS8* transgenic plants and WT (Table 1). Although N deficiency greatly reduced the seed yield per plant (and per square meter), pod number per plant, and seed number per pod of both *BnaC02.TPS8*-OE lines and WT 'ZS11', the above parameters of *BnaC02.TPS8*-OE lines were still significantly greater than WT 'ZS11' at low N (Figure 7f; Table 1). In contrast to the *BnaC02.TPS8*-OE plants, seed yield per square meter, and seed number per pod in *BnaC02.TPS8* mutants were significantly lower than those in 'Westar' (Figure 7f; Table 1). The pod number per plant of *CR-44* mutant was significantly decreased compared with that in WT under both high and low N conditions (Table 1). These indicate that *BnaC02.TPS8* plays a positive role in the seed yield-related traits of *B. napus*.

BnaC02.TPS8 increases seed oil accumulation, but decreases proteins and soluble sugar accumulation

BnaC02.TPS8 is highly expressed in the pods 22 to 42 DAF stage (Figure 1a), which is the critical period for seed oil accumulation and, thus the expression of *BnaC02.TPS8* may influence seed oil and protein accumulation. Compared with the WT, seed oil in *BnaC02.TPS8* mutants and OE lines was reduced by 1.5%-6.4% and increased by 7.4%-8.9%, respectively (Figure 8a). Seed protein concentration was approximately 3% higher in *BnaC02.TPS8* mutants but 10% lower in *BnaC02.TPS8*-OE compared with WT (Figure 8b). Furthermore, the fatty acid (FA) composition in seeds showed that concentrations of C18:1 were higher, and concentrations of C18:0 and C18:2 were lower in the *BnaC02.TPS8*-OE lines compared to their WT (Figure S4). There was no significant difference in FA composition between *BnaC02.TPS8* mutants and WT (Figure S4).

The concentrations of soluble sugar and starch in the pods play a crucial role in seed filling (Bennett et al., 2011). Seed soluble sugar concentration of *BnaC02.TPS8* mutants was significantly higher than that of WT (Figure 8c). In contrast, the soluble sugar

concentration in mature seeds of *BnaC02.TPS8*-OE lines was significantly lower compared to WT (Figure 8c). Moreover, seed starch concentration was lower in *BnaC02.TPS8* mutants but higher in *BnaC02.TPS8*-OE lines (Figure 8d). As compared with their WT, the net photosynthetic rate of developing pods was significantly lower in *BnaC02.TPS8* mutants and was significantly higher in *BnaC02.TPS8*-OE lines (Figure 8e).

Expression of genes related to starch synthesis (*GBSS1* and *GBSS2*) was down-regulated in the *BnaC02.TPS8* mutants and up-regulated in *BnaC02.TPS8*-OE lines in the developing seeds (Figure 8f,g). The genes encoding proteins involved in fatty acid synthesis and transcriptional activators of fatty acid synthesis (*WRI1*, *MCAMT*, and *FATA*) were significantly down-regulated in the *BnaC02.TPS8* mutants and significantly up-regulated in the *BnaC02.TPS8*-OE lines (Figure 8h-j). The expression of genes (*OBO1* and *CALO*) involved in oil storage was significantly lower in *BnaC02.TPS8* mutants and higher in *BnaC02.TPS8-OE* lines compared to their WT (Figure 8k-l). These data indicate that manipulation of *BnaC02.TPS8* can affect seed oil, protein, and soluble sugar accumulation in *B. napus*.

DISCUSSION

Class I TPSs are known to have active TPS enzymes that regulate T6P concentration in plants (Lunn et al., 2006; Paul et al., 2008). In contrast, the functions of class II TPSs in T6P accumulation in crops have been poorly understood. Our study reveals the previously unknown function of *BnaC02.TPS8*, a class II TPS in *B. napus*. *BnaC02.TPS8* increases leaf T6P concentrations, seed yield, and seed oil accumulation by enhancing photosynthesis in mature leaves and developing pods. This discovery highlights *BnaC02.TPS8* as an important class II TPS mediating seed yield improvement in *B. napus*.

Overexpression of *BnaC02.TPS8* enhances seed yield and oil accumulation in *B. napus*

Chemical and genetic T6P modulation can boost crop yield by regulating photosynthesis and assimilate partitioning in crops (Nuccio et al., 2015; Griffiths et al., 2016; Oszvald et al., 2018). In our study, overexpressing *BnaC02.TPS8* significantly increased seed yield under both high and low N conditions, while mutations in *BnaC02.TPS8* significantly decreased seed yield (Figure 7). This aligns with the

findings in rice, where *OsTPS8* mutations reduce seed yield under normal growth conditions (Vishal et al., 2019), emphasizing the positive role of class II TPS in yield formation.

The rainfall can affect the transpiration rate of leaves and, consequently, the seed yield of oilseed rape, particularly during critical developmental stages (Secchi et al., 2023). The precipitation was notably lower from March to May in 2020 compared to the same period in 2018 and 2019. Consequently, the seed yield of both WT and *BnaC02.TPS8*-OE was lower in 2020 than that of those in both 2018 and 2019. However, the seed yield of *BnaC02.TPS8*-OE lines was significantly higher than that of the WT across all three years (Figure 7). These findings demonstrate that *BnaC02.TPS8*-OE lines had higher adaptation during lower rainfall seasons compared with WT. The planting density in rows spaced 30 cm apart is a widely adopted practice in field trials of *B. napus* (Hu et al., 2020; Zhang et al., 2023). In this study, the average seed yield of the commercial *B. napus* cultivar (*cv*. Zhongshuang11, ZS11) was 2738 kg ha^{-1} in 2018, 3365 kg ha^{-1} in 2019, 2546 kg ha^{-1} in 2020 in rows spaced 30 cm apart (Figure 7g). Remarkably, in the same rows spaced, the seed yields of *BnaC02.TPS8*-OE were significantly higher than those of ZS11 across all three years (Figure 7g).

In *B. napus*, the pod (or silique) wall serves as both an important carbohydrate sink and a source of photosynthates for seeds during the seed-filling stage (King et al., 1997; Bennett et al., 2011). *BnaC02.TPS8*, highly expressed in developing pods (Figure 1b), likely contributes to early-stage embryo development. Our study revealed that *BnaC02.TPS8*-OE increased pod photosynthesis, seed and pod number, and overall seed yield, irrespective of soil N levels (Figure 7-8; Table 1). However, the reduced expression of NR, NRT1.5, and GLN11 in the roots of OE lines (Figure 6) suggests a potential compromise in N uptake, correlating with decreased N content in leaves (Figure 2m). It appears that *BnaC02.TPS8* exhibits a preference for responding to inner N concentrations rather than the environmental N availability.

Improving oil production is a central goal in rapeseed breeding (Lu et al., 2011; Hua et al., 2012). As the seeds become more mature, hexose concentrations and soluble acid invertase activity in the pod wall decreases, giving way to starch accumulation in young seeds (King et al., 1997). Our study found that mutating *BnaC02.TPS8* significantly increased soluble sugars and reduced starch in mature seeds, while overexpressing of

BnaC02.TPS8 had the opposite effect (Figure 8b,c). Therefore, *BnaC02.TPS8* seems to promote starch accumulation over sucrose in the seeds, affecting hexose concentrations or enhancing starch degradation in pod wall. To fully understand *BnaC02.TPS8*'s role in photosynthesis and assimilate partitioning between the pod wall and developing seeds during the podding stage, precise quantification of metabolite profiles and gene expression in stems, pod walls, and developing seeds is necessary.

The quantity of starch in seeds is insufficient to meet the demands of oil synthesis, necessitating the continuous import of sucrose and possible seed CO_2 fixation (King et al., 1997). Signals from the pod wall coordinate seed filling and the redistribution of reserves (Bennett et al., 2011). Our study revealed significant reductions in the expression of genes involved in seed fatty acid and oil biosynthesis in *BnaC02.TPS8* mutants and increased expression in *BnaC02.TPS8*-OE lines (Figure 8h-l). Notably, the concentration of oleic acid (18:1) increased, while saturated fatty acid (18:0) decreased in seeds of *BnaC02.TPS8*-OE lines (Figure S4). Consequently, seed oil concentration was lower in mutant lines and higher in overexpressing lines compared to their WT (Figure 8a). Mutation of *BnaC02.TPS8* significantly decreased the expression of the key transcriptional factor *WRI1*, which impacts glycolysis, fatty acid biosynthesis, and lipid metabolism during seed oil accumulation (Cernac and Benning 2004; To et al., 2012). Elevated *WRI1* expression in *BnaC02.TPS8*-OE lines was associated with increased seed oil content compared to the WT (Figure 8a, h). In summary, overexpressing *BnaC02.TPS8* not only increases seed yield but also improves the oil quality of *B. napus*.

BnaC02.TPS8 boosts net photosynthesis by enhancing carbon flux into sucrose and starch

In our study, overexpressing class II TPS *BnaC02.TPS8* resulted in higher net photosynthetic rate and increased expression of sugar transporter genes (Figure 2h; 6g-i), concomitant with augmented sugar accumulation and total TPS activity in leaves (Figure 3;5d). Conversely, *BnaC02.TPS8* mutants displayed lower total TPS activity, leading to reduced sugar transportation and accumulation in leaves (Figure 3;5d;6g-i). T6P is a key regulator of photoassimilate partitioning (Li et al., 2019). Despite class II TPS typically lacking TPS activity (Delorge et al., 2015), we speculate that BnaC02.TPS8 may regulate TPS activity through interactions with itself or other

399 BnTPSs, forming homodimers or heterodimers, similar to the mechanism observed in
400 rice (Zang et al., 2011).
401 It is noteworthy that both AtTPS8 and BnaC02.TPS8 are expressed at the
402 peduncle/pod boundaries of the young pods (Ramon et al., 2009; Figure 1b(3)). Pods
403 are crucial sources of assimilates and nutrients for supporting developing seeds,
404 particularly in the *Brassicaceae* family (Bennett et al., 2011). Compared to the wild
405 type, *BnaC02.TPS8*-OE and *BnaC02.TPS8* mutant pods exhibited significantly
406 increased and decreased net photosynthetic rates, respectively (Figure 8e). Moreover,
407 $BnaC02.TPS8_{pro}$::*GUS* expression patterns showed a stronger presence of
408 *BnaC02.TPS8* in green leaves compared to senescent leaves (Figure 1c), suggesting a
409 role of *BnaC02.TPS8* in controlling C assimilation and photosynthesis in young leaves.
410 Balancing C and N metabolism is essential for optimal plant growth under varying
411 environmental conditions (Han et al., 2020). Notably, overexpression of *BnaC02.TPS8*
412 did not affect total C concentrations but reduced total N concentrations, resulting in
413 higher C/N ratios in *BnaC02.TPS8*-OE lines under sufficient N conditions (Figure 2l-
414 n). Thus, overexpressing *BnaC02.TPS8* appears to stimulate an enhanced N demand
415 and promote C assimilation in transgenic plants.
416 Starch synthesis occurs through ADPG pyrophosphorylase (AGPase) in chloroplasts,
417 allosterically activated by 3-phosphoglycerate (3PGA) (Stitt and Zeeman 2012). In
418 *BnaC02.TPS8* mutants, AGPase activity, 3PGA and ADPG concentrations, and the
419 expression of genes involved in starch synthesis all decreased (Figure 3-6). In contrast,
420 *BnaC02.TPS8*-OE increased AGPase activity, 3PGA and ADPG concentrations. This
421 suggests that *BnaC02.TPS8* can influence metabolite pools in *B. napus* by altering
422 starch accumulation, possibly independent of T6P concentration. AGPase has two small
423 subunits subject to redox regulation, influenced in Arabidopsis by overexpressing the
424 *E. coli* TPS encoding gene (*OtsA*) (Tiessen et al., 2002; Martins et al., 2013). While
425 AGPase activity appears related to *BnaC02.TPS8* (Figure 5c), the impact of
426 *BnaC02.TPS8* on AGPase's *in vivo* redox status remains unclear.
427 The mutation in *BnaC02.TPS8* resulted in an increased C allocation to TCA pathway
428 intermediates, concurrently decreasing allocation to starch, soluble sugars. Conversely,
429 *BnaC02.TPS8*-OE plants exhibited the opposite trend (Figure 3; 4). In *BnaC02.TPS8*
430 mutants, there was an increase in pyruvate and pyruvate kinase, both involved in

glycolysis. In contrast, OE lines showed a decrease in these components (Figure 4c, 5e). The activity of pyruvate kinase reflects the leaf's capacity to regulate glycolysis for respiration and produce C skeletons required for anabolic processes (Plaxton, 1996). The redirection of photoassimilates away from respiratory pathways towards starch synthesis might contribute to the increased starch observed in *BnaC02.TPS8*-OE plants. Previous studies have identified pyruvate kinase as a target of SnRK1 (Beczner et al., 2010), with SnRK1 exerting negative effects on several TCA intermediates, including citrate, aconitate and isocitrate (Peixoto et al., 2021). Our study revealed that *BnaC02.TPS8* mutants exhibited higher concentrations of citrate, aconitate, and isocitrate (Figure 4). These findings suggest that while the impact of SnRK1 on pyruvate kinase activity exhibits opposing effects, its influence on TCA intermediates aligns with the observed effects in *BnaC02.TPS8* mutants. Notably, overexpressing *otsA* under an ethanol-inducible promoter in Arabidopsis led to increased C allocation to organic and amino acids, while decreasing glycolysis intermediates (Figueroa et al., 2016). These may be attributed to the interplay between source and sink in *otsA* overexpressing *Arabidopsis* and *BnaC02.TPS8* overexpressing *B. napus* plants.

The overexpression of *BnaC02.TPS8* resulted in a significant increase in T6P concentrations, whereas knockout lines showed no change in T6P, UDPG, or G6P concentrations compared with WT (Figure 3e,f,i). This suggests that *BnaC02.TPS8* has a limited role in T6P synthesis. The altered total TPS activity in *BnaC02.TPS8*-OE lines or mutant could be a result of feedback regulation from trehalose concentrations or other unidentified mechanisms. Surprisingly, *BnaC02.TPS8*-OE lines had elevated T6P and sucrose concentrations in fully expanded leaves, contradicting the sucrose-T6P model, where elevated T6P is expected to reduce sucrose concentration (Yadav et al., 2014). Similar observations were made in pith and florets of MADS6:*OsTPP1* transgenic maize lines, where pith showed decreased T6P and sucrose concentrations, while florets had low T6P and higher sucrose concentrations (Oszvald et al., 2018). Notably, the negative impact of T6P concentration on SnRK1 activity was observed solely in young leaves, not in mature leaves of *Arabidopsis* (Zhang et al., 2009), indicating that the influence of T6P concentration may vary across different tissues.

The increased sucrose synthesis or decreased consumption in this study could be attributed to secondary effects resulting from the sustained elevation of T6P

concentration or total TPS activity in *BnaC02.TPS8*-OE lines. Recent research by Van Leene et al. (2022) reported that the class II TPS-like protein AtTPS8 functions as a negative regulator of SnRK1 in *Arabidopsis*. To precisely elucidate how SnRK1 affects T6P concentration in the pods and developing seeds, accurate quantification of changes in metabolic fluxes among *BnaC02.TPS8* mutants, OE lines, and wild type using stable isotope labeling is imperative. Furthermore, investigating the relative contributions of plastidial, mitochondrial, and cytosolic pathways to fatty acid biosynthesis will contribute to a comprehensive understanding of *BnaC02.TPS8*'s function in lipid metabolism.

In conclusion, our study reveals the previously unknown function of *BnaC02.TPS8*, a class II TPS in *B. napus*. *BnaC02.TPS8* exhibits specific expression in mature leaves and developing pod walls of *B. napus*. *BnaC02.TPS8* enhances the allocation of photoassimilates to starch and sucrose, favoring seed yield and oil concentration without adverse effects on plant growth and development. This discovery highlights *BnaC02.TPS8* as an important class II TPS mediating seed yield and oil accumulation improvement in *B. napus*, which offer valuable insights for future crop enhancement.

EXPERIMENTAL PROCEDURES

Identification and sequence analysis of *BnaC02.TPS8* in *B. napus*

The *B. napus* sequences of putative homologs of the *Arabidopsis AtTPS8* gene were retrieved through a BLAST search program in BnTIR (http://yanglab.hzau.edu.cn/; Liu et al., 2021). Each of the *BnTPS8* genes was confirmed to be a member of the TPS family using the SMART database (http://smart.embl-heidelberg.de/, Letunic et al., 2018) and NCBI Conserved Domain Search Database (http://www.ncbi.nlm.nih.gov/Structure/cdd/wrpsb.cgi). Protein sequences of BnTPS8 and AtTPS8 were aligned using the ClustalW in MEGA 11 (Tamura et al., 2021). A phylogenetic tree was constructed with the maximum-likelihood method by MEGA 11 using an algorithm with 1000 bootstraps, based on the equal input model, using partial deletion of 95% site coverage for gaps and missing data.

Plant materials and growth conditions

In this study, a commercial *B. napus* cultivar (*cv*. Zhongshuang11, ZS11) was employed for gene cloning, and both the universal cultivar 'Westar' and 'ZS11' were used for the

transformation receptor. Hydroponic experiments were conducted using a modified Hoagland solution (Shi et al., 2013). The pH of the nutrient solutions was adjusted to 5.8 using 2 M NaOH or HCl. The nutrient solution was constantly aerated throughout the experiments and refreshed every three days. Plants were cultivated in an illuminated growth chamber at 22℃ with 60% relative humidity under 16 h: 8 h light/dark regime. To avoid the influence of the circadian rhythm, samples were taken in the middle of the day. The experiments were replicated four to six times.

Three years of field trials were conducted at the experimental site of Huazhong Agricultural University in Wuhan (114.3°E, 30.5°N), Hubei Province, China from October 2017 to May 2020. The soil was a yellow-brown soil (Alfisol), and its properties were as follows: pH6.8 (1:5 soil solution ratio), organic matter 10.70 g kg^{-1}, NH_4OAc-extracted potassium 120.20 mg kg^{-1}, total N (Kjeldahl acid-digestion method) 0.35 g kg^{-1}, available N (alkali-hydrolysable N) 25.60 mg kg^{-1}, and Olsen-P 8.30 mg kg^{-1}. Seeds of transgenic lines and WT were sown in a nursery bed in the field in mid-September and the seedlings were transplanted by hand 30 days after sowing. There were two N treatments, namely (1) high N of 180 kg N ha^{-1} (basal fertilizer 108 kg N ha^{-1}; top dressing 72 kg N ha^{-1}) and low N of 72 kg N ha^{-1} (basal fertilizer 43.2 kg N ha^{-1}, top dressing 28.8 kg N ha^{-1}). All the plots received basal fertilizer, including 60% of the total N applied (supplied as urea), and all the P (supplied as calcium superphosphate), K (supplied as potassium chloride), and boron (supplied as $Na_2B_4O_7 \cdot 10H_2O$). The application rates were as follows: P 90 kg P_2O_5 ha^{-1}, K 120 kg K_2O ha^{-1}, and Borax 15 kg ha^{-1}. These fertilizers were thoroughly mixed and applied in bands near the crop rows. The remaining 40% N was top dressed as urea during overwintering.

A completely randomized block design with three replications was adopted in 2017-2018, 2018-2019, and 2019-2020. The plot size was 6 m length × 1.8 m width, with 0.3 m row spacing and 0.25 m plant spacing, corresponding to 112,500 plants ha^{-1}. Each plot had 6 varieties, and each variety had 3 rows, and 6 plants in each row. Each plot had 20 rows, the first row and the last row were used as guard rows. The plants were grown under rainfed conditions. The monthly average temperature and rainfall during the rapeseed growth seasons were recorded (Figure S4). Weeds, pests, and disease stresses were controlled using spray herbicides, insecticides, and fungicides,

respectively; no obvious weeds, insect pests, or disease infestations occurred during the cropping season (Hu et al., 2020).

Arabidopsis was grown in an environmentally controlled growth room at 22℃. The PAR light intensity of the fluorescent light was 150 μmol m^{-2} s^{-1}. After sterilization, Arabidopsis seeds were sown on agar medium contained with half-strength MS salt, 1.0% (w/v) sucrose, 0.05% MES, and 1.2% (w/v) agar (Sigma-Aldrich Co., St. Louis, MO, catalog no. A1296). After plates were incubated at 4℃ for 2 days, they were transferred to long-day (16 h: 8 h light/dark regime) conditions. Ten-day-old seedlings of *BnaC02.TPS8*pro::GUS were transferred to soil (PINDSTRUP from Denmark, pH5.0) in black plastic pots (10 cm × 10 cm), and sampled at the flowering and pod stage.

Vector construction and plant transformation

To generate the *BnaC02.TPS8*pro::GUS construct, the promoter sequence (*B. napus* cultivar 'ZS11') was inserted into the pBI121-GUS plus vector with a β-glucuronidase (GUS) reporter gene (Li et al., 2015). The complete vector was verified by sequencing and transformed into *Agrobacterium tumefaciens* GV3101 by electroporation. *Arabidopsis* transformation was performed by the floral-dip method (Clough and Bent 1998).

Complete *BnaC02.TPS8* coding sequence (*B. napus* cultivar 'ZS11') was amplified and cloned into the pCAMBIA2300 vector for *B. napus BnaC02.TPS8* overexpression (OE) vectors. To generate the construct for the CRISPR/Cas9 system, two 20 bp target sequences were inserted into the vectors of pKSE401 and pCBC-DT1T2 (Xing et al., 2014). The plasmid constructs were introduced into *Agrobacterium tumefaciens* strain GV3101 by electroporation. Hypocotyls of *B. napus* cultivar 'ZS11' or 'Westar' were transformed (Zhou et al., 2002). The OE lines were confirmed by PCR using specific primers. For the CRISPR/Cas9 mutants, PCR was performed for amplified Cas9, and then the PCR product of the sgRNA target sequence was amplified and sequenced (Wuhan Quintara Biotechnology Co., Ltd). The mutational patterns of CRISPR/Cas9 mutants were analyzed using DSDecode (Liu et al., 2015).

RNA extraction and quantitative RT-PCR (qRT-PCR)

Total RNA was extracted using the EastepR super total RNA extraction kit (Promega, Madison, WI). One μg of total RNA was used to convert into cDNA with the

ReverTrace qPCR RT master mix with gDNA remover (TOYOBO, Osaka, Japan). qRT-PCR was performed using SYBR® green supermix (Bio-Rad) on the CFX Connect Real-Time PCR Detection System (Bio-Rad). The transcript levels were normalized to the housekeeping genes *Tubulin* and *Actin2*.

Subcellular localization

The transiently expressed 35S::BnaC02.TPS8::GFP fusion constructs were introduced into Arabidopsis (Col-0) protoplasts by the PEG/calcium-mediated transformation method (Yoo et al., 2007). The subcellular localization marker construct of m::RFP (red fluorescent protein) was used as a cytosol marker protein (Kim et al., 2016). Fluorescence signals were detected and photographed under a confocal laser microscope (LSM 510 Meta, Carl Zeiss lnc.).

Measurement of biomass, seed yield, and yield-related traits

At the seedling stage, the plants were sampled and divided into shoots and roots. At the ripening stage, the shoot was divided into straw and seeds (almost all the leaves had senesced at this stage). Samples were oven-dried at 105℃ for 30 min, then at 65℃ for 48 h for constant mass. Dried samples were weighed. At the ripening stage, twenty-one plants of each line in three plots were harvested. Among them, seven plants of each line were measured for branch number and pod number per plant. Twenty-five siliques from each plant were sampled randomly and seed numbers were counted. After a subsequent ripening period, all siliques from each plant were threshed and total seed yield and 1000-seed weight were determined. Harvest index = seed yield per plant/ (seed yield + straw weight). The content of seed oil and protein was tested using a near-infrared reflectance spectroscope (Foss NIRSystems 5000) (Gan et al., 2003).

Collection of developing seeds of *B. napus*

Plants were selected at the middle flowering stage, and the 2-3 flowers that had recently opened were pinched off. The main branch and three branches of selected five individual plant replicates of *BnaC02.TPS8*-OE, CRISPR mutants, and WT were labeled with wires, which were gently tied around the stem between the open flower and the bud. The buds of labeled branches were bagged and self-pollinated for 4 days and then the bag was removed. The pods close to the wire were sampled 35 days after flowering (DAF).

GUS histochemical and fluorometric assays

Seedlings or tissues were incubated at 37°C for 6 h in GUS staining solution (1 mM 5-bromo-4-chloro-3-indolyl -β-D-glucuronate acid in 50 mM sodium phosphate buffer, pH7.2) containing 0.1% (v/v) Triton X-100, 0.5 mM $K_4Fe(CN)_6$, 2 mM $K_3Fe(CN)_6$, and 10 mM EDTA. The tissue samples were examined under a stereo-microscope (Olympus, Japan).

Fluorometric GUS assays were conducted in accordance with the method described by Jefferson et al. (1987) with minor adjustments. For quantitative assessments, plant tissues were rapidly frozen and subsequently homogenized in 0.5 mL of GUS extraction buffer, which consisted of 50 mM $NaPO_4$ buffer (pH 7.0), 10 mM EDTA (pH 8.0), 0.1% (w/v) sodium lauryl sarcosine, 0.1% (v/v) Triton X-100, and 10 mM β-mercaptoethanol. The homogenate was then centrifuged at 13,000×g for 15 min at 4℃. GUS activity in the supernatants was quantified in extraction buffer containing 1 mM 4-MUG (4-methylumbelliferyl-β-D-galactopyranoside) at 37℃. A 50 μL aliquot of the supernatant was mixed with 250 μL of MUG assay buffer on ice. Subsequently, 100-μL aliquots were added immediately to 900 μL of GUS stop buffer (0.2 M Na_2CO_3) as a control. The remaining reaction aliquots were incubated at 37℃ for 1 hour, and 100-μL aliquots were then added to 900 μL of the stop buffer. The fluorescence intensity of 4-methylumbelliferone (4-MU) was quantified using a fluorescence spectrophotometer (HITACHI F-4600, Japan) at excitation and emission wavelengths of 365 and 455 nm, respectively. A standard curve was constructed to determine the concentration of 4-MU. The total protein concentration of the crude sample extracts was determined using bovine serum albumin (BSA) as a reference standard. Finally, GUS activity was normalized using the 4-MUG standard and calculated as picomoles of 4-MU produced per minute per milligram of total protein.

In the GUS fluorometric assay of *pBnaC02.TPS8*-GUS Arabidopsis samples, leaf specimens were obtained from leaf 6 at 2, 8, 16 and 22 days after emergence (DAE). Individual flowers on the primary inflorescence were carefully marked at anthesis. Samples were collected from young siliques (5 and 10 days after anthesis) and from mature siliques (20 and 25 days after anthesis). Seeds were meticulously removed using a dissecting needle, and the silique walls and seeds were sampled.

Determination of total C and N concentration

The concentration of total N and C in the dried powder of samples was measured using an elemental analyzer (Vario EL; Elemental analyzer system). C to N ratio (C/N ratio) = total C/ total N.

Measurement of chlorophyll concentration and photosynthetic efficiency

At the seven-week-old stage, the fifth and sixth leaves of the plants were sampled, and fresh leaves (~30 mg) were incubated in 2.5 mL of 80% acetone overnight in the dark at 4℃. Pigment concentration was detected at 663 nm and 645 nm absorbance with a spectrophotometer (Tecan Infinite 200, Switzerland). The concentration of total chlorophyll was calculated using the following equation: $(20.31\ A_{645} + 8.05\ A_{663)}$ / FW [mg g^{-1}] (FW: fresh weight of tissue in grams). The net photosynthesis rate in the middle of leaves at the seedling stage or the pods from the main inflorescence at the podding stage was measured using a portable photosynthesis system (Li6400; LI-COR, Lincoln, NE, USA) with the parameters of 400 μmol mol^{-1} CO_2, 600 μmol s^{-1} flow rate, 60% relative humidity and 1200 μmol m^{-2} s^{-1} light intensity.

Metabolite extraction and analysis by LC-MS/MS

Metabolites (including T6P) were extracted with chloroform/methanol and determined by LC-MS/MS according to a previously described method (Guo et al., 2014; Luo et al., 2007). The 5^{th} and 6^{th} leaves of seven-week-old seedlings were snap-frozen, and ground to powder. Samples (30 mg) were homogenized in 1.8 mL chloroform: methanol (3:7, v/v) containing 0.8 μg PIPES as internal standard and incubated for 2 h with intermittent mixing at -20℃. Polar metabolites were extracted from the methanol/chloroform phase by the addition of 1.6 mL water to each sample and then centrifuged at 12,000 g after vigorous vortexing. The methanol-water phase was then transferred to a new tube. Another 1.6 mL of water was added to each sample to extract polar metabolites one more time. Two extracts were pooled and concentrated using a stream of nitrogen gas in a Termovap sample concentrator (DC150-2, Youning, Hangzhou, China). The extracts were redissolved with 300 μL ddH_2O and then filtered with 0.45 μm cellulose acetate ultrafiltration membranes (Millipore, MA, United States). Metabolites analysis was determined by LC-MS/MS (QTRAP 6500 plus) with the instrumental parameters described by Luo et al. (2007). Six replicates were used for each line. The standard curve for each metabolite was generated using authentic

standards for the quantification of targeted metabolites. Sugar phosphates, glycolytic intermediates, and organic acids were determined by interpolating from the linear relationship between peak area and standard concentration.

Measurement of carbohydrates

Carbohydrates were quantified as described previously (Li and Li, 2013; Li et al., 2022). Dried leaves (~0.1 g) were homogenized in 5 mL of 80% (v/v) hot ethanol for 20 min and filtered for the assays. To measure soluble sugar, the filtrate was boiled for 15 min with anthrone and 98% sulfuric acid. The absorbance was recorded at 485 nm using a spectrophotometer (Tecan Infinite 200, Switzerland). To measure sucrose, the filtrate was boiled for 10 min with 2 N NaOH and then chilled, then 10 N HCl and 0.1% resorcinol were added to the above mixture, and incubated at 80℃ for 10 min. The absorbance was recorded at 480 nm after cooling. For starch quantification, the filtrate was dried, weighed, and sequentially boiled with deionized water, 9.2 M perchloric acid, and 4.6 M perchloric acid, respectively. The mixture was centrifuged at 12,000 g for 20 min. The supernatants were treated using the same procedures as for soluble sugar and measured for absorbance at 485 nm. To measure trehalose, the supernatant was dried at 80℃ and redissolved with distilled water. The re-suspension was sequentially boiled in 0.2 N H_2SO_4 and 0.6 N NaOH. The mixture was treated with anthrone and 98% sulfuric acid at 100℃ for 10 min. The chilled solution was measured for absorbance at 630 nm.

Measurement of trehalose-6-phosphate synthase (TPS) activity

Activity of TPS was measured as the release of UDP from UDP-glucose in the presence of glucose-6-phosphate (Hottiger et al.,1987; Ilhan et al., 2015). Briefly, 0.1 g of fresh leaves were homogenized in 0.4 mL of reaction mixture, containing 50 mM tricine buffer, pH7.0, 10 mM glucose-6-phosphate, 5 mM UDPG, and 12.5 mM $MgCl_2$, and incubated at 35℃ for 30 min. Glucose-6-phosphate was excluded from control experiments. Samples were then kept at 100℃ for 5 min. The mixture was centrifuged at 12,000 g for 10 min. The supernatant was mixed with the second reaction mixture, containing 140 mM tricine, pH 7.6, 2 mM phosphoenolpyruvate, 0.31 mM NADH, and 20 U lactic dehydrogenase, for determination of UDP content. The reaction was started by the addition of pyruvate kinase (20 U). A decrease in absorbance at 340 nm was measured at 35℃, and used to calculate the concentration of UDP. One unit of enzyme activity was defined as nmol UDP formed through the activity of TPS in the extract,

and total shoot enzyme activity was expressed as units g^{-1} fresh weight.

Measurement of sucrose phosphate synthase, invertase, sucrose synthase, AGPase and cytosolic pyruvate kinase activity

Sucrose phosphate synthase activity was measured according to Nägele et al. (2010). Frozen leaf tissue was homogenized in 50 mM HEPES-KOH (pH 7.5), 15 mM $MgCl_2$, 1 mM EDTA, 2.5 mM DTT, and 0.1% Triton X-100. After centrifugation at 12,000 g for 5 min at 4°C, SPS activity in the supernatant was determined. The reaction buffer consisted of 50 mM HEPES-KOH, pH 7.5, 15 mM $MgCl_2$, 2.5 mM DTT, 10 mM UDP-Glc, 10 mM Fru-6-P, and 40 mM Glc-6-P. Control assays included 30% KOH. Reactions were performed at 25°C for 30 min, followed by a 10 min incubation at 95°C. Anthrone (0.2%) in 95% H_2SO_4 was added, and samples were incubated for 8 min at 90°C. Glucose concentration was measured at 620 nm.

Invertase activities were evaluated in crude leaf extracts. Approximately 0.1 g of frozen leaf tissues was homogenized in 50 mM HEPES-KOH (pH 7.5), 5 mM $MgCl_2$, 1 mM EDTA, 1 mM EGTA, 1 mM PMSF, 5 mM DTT, 0.1% Triton X-100, and 10% glycerin. After centrifugation at 12,000 g for 25 min at 4°C, invertase activities were assayed in the supernatant. Soluble acid invertase was assayed in 20 mM Na-acetate buffer (pH 4.7) with 100 mM sucrose as a substrate. Neutral invertase was assayed in 20 mM HEPES-KOH (pH 7.5) with 100 mM sucrose as a substrate. The control of each assay was boiled for 3 min after adding the enzyme extract. Reactions were incubated for 60 min at 30°C, stopped by boiling for 3 min, and the reducing sugars released were enzymatically measured (Comin Biotechnology Co., Ltd.). The activities were expressed in μmol glucose h^{-1} g^{-1} FW.

To assay sucrose synthase activity, frozen samples were ground to powder and then homogenized in extraction buffer containing 50 mM HEPES/KOH (pH7.5), 7.5 mM $MgCl_2$ and 1 mM EDTA, 2% (w/v) PEG 8000, 2% (w/v) PVP and 5 mM DTT (Hoffmann-Thoma et al., 1996). The supernatant was immediately desalted on a Sephadex G-25 column equilibrated with extraction buffer at 4°C. The filtrate was then used to determine the sucrose synthase activities with a test kit (Comin Biotechnology Co., Ltd.).

To assay AGPase enzyme activity, frozen samples were ground to powder and then homogenized in extraction buffer containing 1 mL extraction buffer consisting of

100 mM HEPES buffer (pH 7.5), 5 mM $MgCl_2$, 2 mM EDTA, 10% (v/v) glycerol, 0.1% BSA, 5 mM DTT, and 2% (w/v) insoluble PVP, and then centrifuged at 12,000 g at 4°C for 30 min. The remaining pellet was suspended in the extraction buffer and used for AGPase enzyme assay with a test kit (AGP-2A-Y, Comin Biotechnology Co., Ltd.).

Crude pyruvate kinase enzyme solutions were extracted following Baud et al. (2007). Leaves were ground and homogenized in extraction buffer (50 mM HEPES-KOH, pH 8.0, 100 mM KCl, 5 mM $MgCl_2$, 20 mM NaF, 1 mM EDTA, 0.1% Triton X-100, 20% glycerol, 5% PEG 8000, 1 mM DTT, 1% PVP). The supernatant obtained after centrifugation at 14,000 g at 4°C for 10 min was used for enzyme activity. The assay involved a coupling reaction of pyruvate and the conversion of NADH to NAD^+. The reaction solution (100 mM HEPES-KOH, pH 8.2, 50 mM KCl, 10 mM $MgCl_2$, 5% PEG 8000, 1 mM DTT, 2 mM PEP, 0.3 mM NADH, 2.5 mM ADP, 2 U/mL rabbit muscle lactate dehydrogenase) was analyzed for pyruvate kinase activity by monitoring the decrease in absorbance values at 340 nm.

Data analysis and statistics

Data were processed using SPSS software 22.0 (IBM Corp.). The heatmap and bar chart were completed by Microsoft Excel software and GraphPad 8.0 software (GraphPad, USA), respectively. A two-tailed Student's *t*-test was performed to identify significant differences between WT and transgenic plants for physiological data.

ACKNOWLEDGMENTS

This work was supported by the National Nature Science Foundation of China (Grant Nos. 32301885, 31972498, and 32172662). Pan Yuan gratefully acknowledges financial support from the China Scholarship Council to Reading University for joint doctoral student education. We thank Prof. Liang Guo and Ms. Qing Li (Huazhong Agricultural University) for their excellent technical assistance in metabolite analysis by LC-MS/MS.

Supplemental Data

Figure S1. Multiple sequence alignment of AtTPS8, BnaC02.TPS8 and BnaA02.TPS8 proteins and structure similarity in *B. napus* and *Arabidopsis*. The red striated bar indicates the Glyco_transf_20 domain (Glycosyltransferase family 20,

https://www.ncbi.nlm.nih.gov/Structure/cdd/pfam00982). The green striated bar indicates the Trehalose_PPase domain (Trehalose-phosphatase domain, https://www.ncbi.nlm.nih.gov/Structure/cdd/PF02358).

Figure S2. GUS activity in *pBnaC02.TPS8*-GUS Arabidopsis. GUS activity was measured in Arabidopsis plants expressing the *pBnaC02.TPS8*-GUS construct. Leaf samples were collected at 2, 8, 16, and 22 days after emergence (DAE), while pod walls and seeds were sampled at 5, 10, 20, and 25 days after anthesis (DAA). Data are shown as the mean ± SD (n=4). Different letters represent significant differences at $P < 0.05$, based on an ANOVA analysis with Tukey's significant difference test.

Figure S3. Comparison of shoot growth among different six-week-old *BnaC02.TPS8-OE* lines and wild type plants (cultivar 'ZS11') grown hydroponically. Values are the means ± SD (n=5). Different letters represent significant differences at $P < 0.05$, based on an ANOVA analysis with Tukey's significant difference test.

Figure S4. Climate conditions during rapeseed growth seasons (2017-2020). Monthly averages of maximum and minimum temperatures, along with precipitation data, are depicted for the rapeseed growth seasons spanning 2017 to 2020.

Figure S5. Impact of *BnaC02.TPS8* on the sugar-phosphates of leaves. (a-c) Concentrations of F6P (a), F1,6BP (b), and G1P (c) in seven-week-old seedlings of WT, *BnaC02.TPS8* mutants (CR-44 and CR-153; WT, 'Westar') and overexpression lines (OE-33 and OE-38; WT, 'ZS11'). Data were obtained from the 5^{th} and 6^{th} leaves of seven-week-old seedlings grown hydroponically. Data are shown as the mean ± SD (n=6). Significant differences: $*P < 0.05$, $**P < 0.01$ and ns indicates not significant (Student's *t*-test).

Figure S6. Impact of *BnaC02.TPS8* on the fatty acid composition in mature seeds. (a-f) Fatty acid composition, including C16:0 (a), C18:0 (b), C18:1 (c), C18:2 (d), C18:3 (e) and C20:0 (f) in mature seeds of WT, *BnaC02.TPS8* mutants (CR-44 and CR-153; WT, 'Westar'), and overexpression lines (OE-33 and OE-38; WT, 'ZS11'). Data were measured by a near-infrared spectrometer (NIRS). Data are shown as the mean ± SD (n=7). Significant differences: $*P < 0.05$ and ns indicates not significant (Student's *t*-test).

Table S1 The sequences of putative off-target sites of *BnaA02.TPS8* in *BnaC02.TPS8* CRISPR-Cas9 mutants.

Table S2 Abundance changes in metabolites of *BnaC02.TPS8* overexpression lines and mutants by LC-MS/MS.

Table S3 Primers used for *BnaC02.TPS8* cloning and vector construction.

Table S4 Primers used for qRT-PCR of reference genes, *BnaC02.TPS8*, *BnaA02.TPS8*, and genes associated with starch synthesis, starch degradation, sugar metabolites transport, nitrogen uptake and metabolism, fatty acid synthesis, and oil storage.

AUTHOR CONTRIBUTIONS

L.S. and P.Y. conceived and designed the experiments; P.Y. performed most of the experiments, analyzed the data, and drafted the manuscript; G.Z.L. provided technical assistance; M.Z.Y. and H.J.L. collected the samples and worked on the phenotyping; J.P.H., D.F.H., H.M.C., G.D.D., S.L.W., F.S.X., and C.W. revised the manuscript. All authors provided final approval for publication.

CONFLICT OF INTEREST

The authors declare that they have no competing interests.

REFERENCES

Arnon DI (1949) Copper enzymes in isolated chloroplasts. Polyphenoloxidase in *Beta vulgaris*. Plant Physiol **24,** 1-15

Baud S, Wuillème S, Dubreucq B, de Almeida A, Vuagnat C, Lepiniec L, Miquel, M, Rochat C (2007) Function of plastidial pyruvate kinases in seeds of *Arabidopsis Thaliana*. Plant J **52,** 405-419

Bennett EJ, Roberts JA, Wagstaff C (2011) The role of the pod in seed development: strategies for manipulating yield. New Phytol **190,** 838-853

Cabib E, Leloir LF (1958) The biosynthesis of trehalose phosphate. J Bio Chem **231,** 259-275

Cernac A, Benning C (2004) WRINKLED1 encodes an AP2/EREB domain protein involved in the control of storage compound biosynthesis in *Arabidopsis*. Plant J **40(4),** 575-585

Chary SN, Hicks GR, Choi YG, Carte D, Raikhel NV (2008) Trehalose-6-phosphate synthase/phosphatase regulates cell shape and plant architecture in *Arabidopsis*. Plant Physiol **146,** 97-107

Clough SJ, Bent AF (1998) Floral dip: a simplified method for *Agrobacterium*-mediated transformation of *Arabidopsis thaliana*. Plant J **16,** 735-743

Damgaard O, Jensen LH, Rasmussen OS (1997) *Agrobacterium tumefaciens*-mediated transformation of *Brassica napus* winter cultivars. Transgenic Res **6,** 279-288

De Block M, De Brouwer D, Tenning P (1989) Transformation of *Brassica napus* and *Brassica oleracea* using *agrobacterium tumefaciens* and the expression of the *bar* and *neo* genes in the transgenic plants. Plant Physiol **91(2),** 694-701

Delorge I, Figueroa CM, Feil R, Lunn JE, Van Dijck P (2015) Trehalose-6-phosphate synthase 1 is not the only active TPS in *Arabidopsis thaliana*. Biochem J **466,** 283-290

Eastmond PJ, van Dijken AJ, Spielman M, Kerr A, Tissier AF, Dickinson HG, Jones JD, Smeekens SC, Graham IA (2002) Trehalose-6-phosphate synthase 1, which catalyzes the first step in trehalose synthesis, is essential for *Arabidopsis* embryo maturation. Plant J **29,** 225-235

Figueroa CM, Feil R, Ishihara H, Watanabe M, Kölling K, Krause U, Höhne M, Encke B, Plaxton WC, Zeeman SC, Li Z, Schulze WX, Hoefgen R, Stitt M, Lunn JE (2016) Trehalose 6-phosphate coordinates organic and amino acid metabolism with carbon availability. Plant J **85,** 410-423

Figueroa CM, Lunn JE (2016) A tale of two sugars: trehalose 6-phosphate and sucrose. Plant J **172,** 7-27

Food and Agriculture Organization of the United Nations (FAO) (2020) The state of food security and nutrition in the world 2020. Transforming food systems for affordable healthy diets. FAO, Rome, Italy. http://www.fao.org/faostat

Gan L, Sun XL, Jin L, Wang GQ, Xu JW, Wei ZL, Fu TD (2003) Establishment of math models of NIRS analysis for oil and protein contents in seed of *Brassica napus*. Scientia Agricultura Sinica **36(12),** 1609-1613

Gómez LD, Baud S, Gilday A, Li Y, Graham IA (2006) Delayed embryo development in the *Arabidopsis TREHALOSE-6-PHOSPHATE SYNTHASE 1* mutant is associated with altered cell wall structure, decreased cell division and starch accumulation. Plant J **46,** 69-84

Griffiths CA, Sagar R, Geng Y, Primavesi LF, Patel MK, Passarelli MK, **Gilmore IS, Steven RT, Bunch J, Paul MJ, et al.** (2016) Chemical intervention in plant sugar signalling increases yield and resilience. Nature **540,** 574-578

Guo L, Ma F, Wei F, Fanella B, Allen DK, Wang X (2014) Cytosolic phosphorylating glyceraldehyde-3-phosphate dehydrogenases affect *Arabidopsis* cellular metabolism and promote seed oil accumulation. Plant Cell **26 (7),** 3023-3035

Han X, Wu K, Fu X, Liu Q (2020) Improving coordination of plant growth and nitrogen metabolism for sustainable agriculture. aBIOTECH **(4),** 255-275

Hendriks JH, Kolbe A, Gibon Y, Stitt M, Geigenberger P (2003) ADP-glucose pyrophosphorylase is activated by posttranslational redox-modification in response to light and to sugars in leaves of *Arabidopsis* and other plant species. Plant Physiol **133,** 838-849

Henry C, Bledsoe SW, Siekman A, Kollman A, Waters BM, Feil R, Stitt M, Lagrimini LM (2014) The trehalose pathway in maize: conservation and gene regulation in response to the diurnal cycle and extended darkness. J Exp Bot **65,** 5959-5973

Hottiger T, Schmutz P, Wiemken A (1987) Heat-induced accumulation and futile cycling of trehalose in *Saccharomyces cerevisiae*. J Bacteriol **169,** 5518-5522

Hu W, Lu Z, Meng F, Li X, Cong R, Ren T, Sharkey TD, Lu J (2020) The reduction in leaf area precedes that in photosynthesis under potassium deficiency: the importance of leaf anatomy. New Phytol **227,** 1749-1763

Hua W, Li R J, Zhan GM, Liu J, Li J, Wang XF, Liu GH, Wang HZ (2012) Maternal control of seed oil content in *Brassica napus*: the role of silique wall photosynthesis. Plant J **69(3),** 432-444

Ilhan S, Ozdemir F, Bor M (2015) Contribution of trehalose biosynthetic pathway to drought stress tolerance of *Capparis ovata* Desf. Plant Biol **17,** 402-407

Jefferson RA, Kavanagh TA, Bevan MW (1987) GUS fusions: beta-glucuronidase as a sensitive and versatile gene fusion marker in higher plants. EMBO J **6,** 3901-3907

Jones TL, Ort DR (1997) Circadian regulation of sucrose phosphate synthase activity in tomato by protein phosphatase activity. Plant Physiol **113,** 1167-1175

Kim RJ, Kim HJ, Shim D, Suh MC (2016) Molecular and biochemical characterizations of the monoacylglycerol lipase gene family of *Arabidopsis thaliana*. Plant J **85,** 758-771

King SP, Lunn JE, Furbank RT (1997) Carbohydrate content and enzyme metabolism in developing canola siliques. Plant Physiol **114,** 153-160

Kolbe A, Tiessen A, Schluepmann H, Paul M, Ulrich S, Geigenberger P (2005) Trehalose 6-phosphate regulates starch synthesis via posttranslational redox activation of ADP-glucose pyrophosphorylase. Proc Natl Acad Sci U S A **102(31),** 11118-11123

Letunic I, Bork P (2018) 20 years of the SMART protein domain annotation resource. Nucleic Acids Res **46(D1),** 493-496

Leyman B, Van Dijck P, Thevelein JM (2001). An unexpected plethora of trehalose biosynthesis

genes in *Arabidopsis thaliana*. Trends Plant Sci **6,** 510-513

Li Q, Shao J, Tang S, Shen Q, Wang T, Chen W, Hong Y (2015) Wrinkled1 accelerates flowering and regulates lipid homeostasis between oil accumulation and membrane lipid anabolism in *Brassica napus*. Front Plant Sci **6,** 1015

Li Q, Yin M, Li Y, Fan C, Yang Q, Wu J, Zhang C, Wang H. Zhou Y (2015) Expression of *Brassica napus TTG2*, a regulator of trichome development, increases plant sensitivity to salt stress by suppressing the expression of auxin biosynthesis genes. J Exp Bot **66,** 5821-5836

Li X, and Li J (2013) Determination of the content of soluble sugar in sweet corn optimized anthrone colorimetric method. Storage Process **13,** 24-27

Li Y, Wang W, Feng Y, Tu M, Wittich PE, Bate NJ (2019) Transcriptome and metabolome reveal distinct carbon allocation patterns during internode sugar accumulation in different sorghum genotypes. Plant Biotechnol J **17(2),** 472-487

Li Z, Wei X, Tong X, Zhao J, Liu X, Wang H, Tang L, Shu Z, Li G, Wang Y, Ying J, Jiao G, Hu H, Hu P, Zhang J (2022) The OsNAC23-T6P-SnRK1a feed-forward loop regulates sugar homeostasis and grain yield in rice. Mol Plant **15,** 706-722

Liu D, Yu L, Wei L, Yu P, Wang J, Zhao H, Zhang Y, Zhang S, Yang Z, Chen G, Yao X, Yang Y, Zhou Y, Wang X, Lu S, Dai C, Yang QY, Guo L (2021) BnTIR: an online transcriptome platform for exploring RNA-seq libraries for oil crop *Brassica napus*. Plant Biotechnol J **19(10),** 1895-1897

Liu J, Hua W, Yang HL, Zhan GM, Li RJ, Deng LB, Wang XF, Liu GH, Wang HZ (2012) The *BnGRF2* gene (GRF2-like gene from *Brassica napus*) enhances seed oil production through regulating cell number and plant photosynthesis. J Exp Bot **63(10),** 3727-3740

Liu W, Xie X, Ma X, Li J, Chen J, Liu YG (2015) DSDecode: a web-based tool for decoding of sequencing chromatograms for genotyping of targeted mutations. Mol Plant **8(9),** 1431-1433

Lu C, Napier JA, Clemente TE, Cahoon EB (2011) New frontiers in oilseed biotechnology: meeting the global demand for vegetable oils for food, feed, biofuel, and industrial applications. Curr Opin Biotechnol **22(2),** 252-259

Lu S, Liu H, Jin C, Li Q, Guo L (2019) An efficient and comprehensive plant glycerolipids analysis approach based on high performance liquid chromatography-quadrupole time-of-flight mass spectrometer. Plant Direct **3,** 1-13

Luo B, Groenke K, Takors R, Wandrey C, Oldiges M (2007) Simultaneous determination of multiple intracellular metabolites in glycolysis, pentose phosphate pathway and tricarboxylic acid cycle by liquid chromatography-mass spectrometry. J Chromatogr A **1147(2),** 153-164

Martins MC, Hejazi M, Fettke J, Steup M, Feil R, Krause U, Arrivault S, Vosloh D, Figueroa CM, Ivakov A, Yadav UP, Piques M, Metzner D, Stitt M, Lunn JE (2013) Feedback inhibition of starch degradation in *Arabidopsis* leaves mediated by trehalose 6-phosphate. Plant Physiol **163(3),** 1142-1163

Morales-Herrera S, Jourquin J, Coppé F, López-Galvis L, De Smet T, Safi A, Njo MF, Griffiths CA, Sidda JD, Mccullagh JS, Xue X, Davis BG, Van der Eycken J, Paul MJ, van Dijck P, Beeckman T (2023) Trehalose-6-phosphate signaling regulates lateral root formation in *Arabidopsis thaliana*. PNAS **120 40,** e2302996120

Nuccio ML, Wu J, Mowers R, Zhou HP, Meghji M, Primavesi LF, Paul MJ, Chen X, Gao Y, Haque E, Haque E, Basu SS, Lagrimini LM (2015) Expression of trehalose-6-phosphate phosphatase in maize ears improves yield in well-watered and drought conditions. Nat Biotechnol **33,** 862-869

Oszvald M, Primavesi LF, Griffiths CA, Cohn J, Basu SS, Nuccio ML, Paul MJ (2018) Trehalose 6-phosphate regulates photosynthesis and assimilate partitioning in reproductive tissue. Plant Physiol **176,** 2623-2638

Paul MJ, Miret JA, Griffiths CA (2022) Improving rice photosynthesis and yield through trehalose 6-phosphate signaling. Mol Plant **15,** 586-588

Paul MJ, Watson A, Griffiths CA (2020) Trehalose 6-phosphate signalling and impact on crop yield. Biochem Soc Trans **48,** 2127-2137

Pellny TK, Ghannoum O, Conroy JP, Schluepmann H, Smeekens S, Andralojc J, Krause KP, Goddijn O, Paul MJ (2004) Genetic modification of photosynthesis with *E. coli* genes for trehalose synthesis. Plant Biotechnol J **2,** 71-82

Ramon M, De Smet I, Vandesteene L, Naudts M, Leyman B, Van Dijck P, Rolland F, Beeckman T, Thevelein JM (2009) Extensive expression regulation and lack of heterologous enzymatic activity of the Class II trehalose metabolism proteins from *Arabidopsis thaliana*. Plant Cell Environ **32,** 1015-1032

Ruan YL (2014) Sucrose metabolism: gateway to diverse carbon use and sugar signaling. Annu Rev Plant Biol **65,** 33-67

Secchi MA, Fernandez JA, Stamm MJ, Durrett T, Prasad PV, Messina CD, Ciampitti I A (2023). Effects of heat and drought on canola (*Brassica napus* L.) yield, oil, and protein: A meta-analysis. Field Crops Res **293,** 108848

Schluepmann H, van Dijken A, Aghdasi M, Wobbes B, Paul M, Smeekens S (2004) Trehalose mediated growth inhibition of *Arabidopsis* seedlings is due to trehalose-6-phosphate accumulation. Plant Physiol **135,** 879-890

Singh V, Louis J, Ayre BG, Reese JC, Pegadaraju V, Shah J (2011) *TREHALOSE PHOSPHATE SYNTHASE11*-dependent trehalose metabolism promotes *Arabidopsis thaliana* defense against the phloem-feeding insect *Myzus persicae*. Plant J **67,** 94-104

Shi L, Shi T, Broadley MR, White PJ, Long Y, Meng J, Xu F, Hammond JP (2013) High-throughput root phenotyping screens identify genetic loci associated with root architectural traits in *Brassica napus* under contrasting phosphate availabilities. Ann Bot **112(2),** 381-389

Stitt M, Zeeman SC (2012) Starch turnover: pathways, regulation and role in growth. Curr Opin Plant Biol **15(3),** 282-292

Suzuki N, Bajad S, Shuman J, Shulaev V, Mittler R (2008) The transcriptional co-activator *MBF1c* is a key regulator of thermotolerance in *Arabidopsis thaliana*. J Bio Chem **283,** 9269-9275

Tan H, Yang X, Zhang F, Zheng X, Qu C, Mu J, Fu F, Li J, Guan R, Zhang H, Wang G, Zuo J (2011) Enhanced seed oil production in canola by conditional expression of *Brassica napus* LEAFY COTYLEDON1 and LEC1-LIKE in developing seeds. Plant Physiol **156 (3),** 1577-1588

Tamura K, Stecher G, Kumar S (2021) MEGA11: Molecular evolutionary genetics analysis version 11. Mol Biol Evol **38(7),** 3022-3027

Tang S, Peng F, Tang Q, Liu Y, Xia H, Yao X, Lu S, Guo L (2022) *BnaPPT1* is essential for chloroplast development and seed oil accumulation in *Brassica napus*. J Adv Res **42,** 29-40

Tian L, Xie Z, Lu C, Hao X, Wu S, Huang Y, Li D, Chen, L (2019) The trehalose-6-phosphate synthase *TPS5* negatively regulates ABA signaling in *Arabidopsis thaliana*. Plant Cell Rep **38,** 869-882

Tiessen A, Hendriks JH, Stitt M, Branscheid A, Gibon Y, Farré EM, Geigenberger P (2002) Starch synthesis in potato tubers is regulated by post-translational redox modification of

ADP-glucose pyrophosphorylase: a novel regulatory mechanism linking starch synthesis to the sucrose supply. Plant Cell **14(9),** 2191-213

To A, Joubès J, Barthole G, Lécureuil A, Scagnelli A, Jasinski S, Lepiniec L, Baud S (2012) WRINKLED transcription factors orchestrate tissue-specific regulation of fatty acid biosynthesis in *Arabidopsis*. Plant Cell **24(12),** 5007-5023

Van Leene J, Eeckhout D, Gadeyne A, Matthijs C, Han C, De Winne N, Persiau G, Van De Slijke E, Persyn F, Mertens T, Smagghe W, Crepin N, Broucke E, Van Damme D, Pleskot R, Rolland F, De Jaeger G (2022) Mapping of the plant SnRK1 kinase signalling network reveals a key regulatory role for the class II T6P synthase-like proteins. Nat Plants **8(11),** 1245-1261

Vigeolas H, Waldeck P, Zank T, Geigenberger P (2007) Increasing seed oil content in oil-seed rape (*Brassica napus* L.) by over-expression of a yeast glycerol-3- phosphate dehydrogenase under the control of a seed-specific promoter. Plant Biotechnol J **5(3),** 431-441

Vishal B, Krishnamurthy P, Ramamoorthy R, Kumar PP (2019) *OsTPS8* controls yield-related traits and confers salt stress tolerance in rice by enhancing suberin deposition. New Phytol **221,** 1369-1386

Wahl V, Ponnu J, Schlereth A, Arrivault S, Langenecker T, Franke A, Feil R, Lunn JE, Stitt M, Schmid M (2013) Regulation of flowering by trehalose-6-phosphate signaling in *Arabidopsis thaliana*. Science **339,** 704-707

Weselake RJ, Shah S, Tang M, Quant PA, Snyder CL, Furukawa-Stoffer TL, Zhu W, Taylor DC, Zou J, Kumar A, Hall L, Laroche A, Rakow G, Raney P, Moloney MM, Harwood JL (2008) Metabolic control analysis is helpful for informed genetic manipulation of oilseed rape (*Brassica napus*) to increase seed oil content. J Exp Bot **59 (13),** 3543-3549

Woodfield HK, Fenyk S, Wallington E, Bates RE, Brown A, Guschina IA, Marillia EF, Taylor DC, Fell D, Harwood JL, Fawcett T (2019) Increase in lysophosphatidate acyltransferase activity in oilseed rape (*Brassica napus*) increases seed triacylglycerol content despite its low intrinsic flux control coefficient. New Phytol **224,** 700-711

Wingler A, Delatte TL, O'Hara LE, Primavesi LF, Jhurreea D, Paul MJ, Schluepmann H (2012) Trehalose 6-phosphate is required for the onset of leaf senescence associated with high carbon availability. Plant Physiol **158,** 1241-1251

Xing HL, Dong L, Wang ZP, Zhang HY, Han CY, Liu B, Wang XC, Chen QJ (2014) A

CRISPR/Cas9 toolkit for multiplex genome editing in plants. BMC Plant Biol **14,** 327-338

Yadav UP, Ivakov A, Feil R, Duan GY, Walther D, Giavalisco P, Piques M, Carillo P, Hubberten HM, Stitt M, Lunn JE (2014) The sucrose-trehalose 6-phosphate (T6P) nexus: specificity and mechanisms of sucrose signalling by T6P. J Exp Bot **65,** 1051-1068

Yang NM, Li S, Wang SL, Li Q, Xu FS, Shi L, Wang C, Ye XS, Cai HM, Ding GD (2020) Dynamic transcriptome analysis indicates extensive and discrepant transcriptomic reprogramming of two rapeseed genotypes with contrasting NUE in response to nitrogen deficiency. Plant and Soil **456,** 369-390

Yoo SD, Cho YH, Sheen J (2007) Arabidopsis mesophyll protoplasts: a versatile cell system for transient gene expression analysis. Nat Protoc **2,** 1565-1572

Zang B, Li H, Li W, Deng XW, Wang X (2011) Analysis of trehalose-6-phosphate synthase (TPS) gene family suggests the formation of TPS complexes in rice. Plant Mol Bio **76,** 507-522

Zhang BB, Wang YJ, Liu HJ, Yang XY, Yuan P, Wang C, Cai HM, Wang SL, Ding GD, Xu FS, Shi L (2023) Optimal phosphorus management strategies to enhance crop productivity and soil phosphorus fertility in rapeseed-rice rotation. Chemosphere **337,** 139392

Zhang D, Zhang H, Hu Z, Chu S, Yu K, Lv L, et al. (2019) Artificial selection on *GmOLEO1* contributes to the increase in seed oil during soybean domestication. PLoS Genet **15(7),** e1008267

Zhang Y, Primavesi LF, Jhurreea D, Andralojc PJ, Mitchell RA, Powers SJ, Schluepmann H, Delatte T, Wingler A, Paul MJ (2009) Inhibition of SNF1-related protein kinase1 activity and regulation of metabolic pathways by trehalose-6-phosphate. Plant Physiol **149,** 1860-1871

Zhou Y, Wang H, Gilmer S, Whitwill S, Keller W, Fowke LC (2002) Control of petal and pollen development by the plant cyclin-dependent kinase inhibitor *ICK1* in transgenic *Brassica* plants. Planta **215,** 248-257

Table 1 Seed yield components and harvest index of *BnaC02.TPS8* mutants (CR-44 and CR-153; WT, Westar) and *BnaC02.TPS8* overexpression plants (OE-33 and OE-38; WT, ZS11) under high and low nitrogen conditions.

	High nitrogen			Low nitrogen			High nitrogen			Low nitrogen		
	Westar	CR-44	CR-153	Westar	CR-44	CR-153	ZS11	OE-33	OE-38	ZS11	OE-33	OE-38
PN (n)	472.5±31.9 a	338.2±32.1 b	398.2±28.1 ab	115.2±12.4 c	85.3±11.3 d	75.8±10.4 d	510.4±59.8 b	709.6±78.8 a	729.3±79.1 a	283.1±38.4 d	403.0±21.2 c	438.5±53.5 c
SN (n)	12.6±0.1 a	10.9±0.2 b	10.7±0.3 b	7.5±0.2 c	4.2±0.2 d	3.6±0.1 d	11.9±0.2 b	13.4±0.4 a	13.2±0.4 a	8.7±0.3 c	10.2±0.4 b	10.3±0.4 b
TSW (g)	4.04±0.06 a	3.91±0.08 a	3.94±0.06 a	3.95±0.05 a	3.94±0.04 a	3.93±0.05 a	4.27±0.04 a	4.29±0.07 a	4.25±0.07 a	4.18±0.02 a	4.25±0.02 a	4.22±0.03 a
HI (n)	2.85±0.10 a	2.97±0.11 a	3.04±0.12 a	2.99±0.14 a	2.89±0.08 a	2.75±0.11 a	3.31±0.05 a	3.39±0.08 a	3.26±0.12 a	2.98±0.11 a	3.12±0.10 a	3.08±0.09 a

Note: PN, pod number of plant; SN, seed number per pod, TSW, thousand seed weight; HI, harvest index. Values are mean ± SD (n=7). Different letters represent significant differences at $P < 0.05$ among treatments, based on an ANOVA analysis with Tukey's multiple comparisons test.

FIGURE LEGENDS

Figure 1. Gene expression pattern, protein localization, and generation of CRISPR/Cas9 mutants, and overexpression transgenic plants of *BnaC02.TPS8*. (a) Phylogenetic tree and gene expression pattern of *BnaC02.TPS8* in *B. napus*. Gene expression data were sourced from BnTIR (http://yanglab.hzau.edu.cn). At, *Arabidopsis thaliana*; Bn, *Brassica napus*. (b) Expression pattern of the *pBnaC02.TPS8* reporter gene in green stem leaf (1) and senescent rosette leaf (2) of post-flowering stage plants, and green silique (3) and yellow silique (4) of silique stage plants. Scale bars: 1 cm. (c) Subcellular localization of BnaC02.TPS8-GFP in *Arabidopsis* protoplast. GFP indicates the green fluorescent protein (GFP) fluorescence, while red indicates the cytosol marker fluorescence. Scale bars: 10 μm. (d) Mutagenesis of target sequence guided by 1 and 2 of the *BnaC02.TPS8* gene. (e) Relative gene expression of *BnaC02.TPS8* in *B. napus* shoots of wild type (cultivar 'ZS11') and *BnaC02.TPS8* overexpression (OE) lines. *BnaEF1-α* and *BnaActin2* were used as the references. Values are the means ± SD (n=4). Significant differences: $^{**}P < 0.01$ (Student's *t*-test).

Figure 2. Impact of *BnaC02.TPS8* disruption on the growth of *B. napus*. (a-b) Growth phenotype of five-week-old seedlings of CRISPR/Cas9 mutants (CR-44 and CR-153; WT, 'Westar') and overexpression lines (OE-33 and OE-38; WT, 'ZS11') grown hydroponically. Scale bars: 2 cm. (c-e) Shoot biomass (c), root biomass (d), and root-to-shoot ratio (e) of seven-week-old seedlings of WT, *BnaC02.TPS8* mutants and overexpression lines. (f-g) Leaf length (f) and leaf width (g) of the 5th leaf of the seven-week-old seedlings. (h-n) Net photosynthetic rate (h), transpiration rate (i), stomatal conductance (j), and intercellular CO2 (k) measured in ten-week-old seedlings grown hydroponically. (l-n) Total carbon (l), total nitrogen (m), and C/N ratio (n) measured in the 5th and 6th leaves of the seven-week-old seedlings. The data in (c-n) are shown as the mean ± SD (n=6). Significant differences: $^{*}P < 0.05$, $^{**}P < 0.01$ and ns indicates not significant (Student's *t*-test).

Figure 3. Impact of *BnaC02.TPS8* on the concentration of sugars, starch, sugar-phosphates, and sugar-nucleotides in the leaves. (a-i) Concentrations of sucrose (a), soluble sugar (b), trehalose (c), starch (d), T6P (e), G6P (f), S6P (g), ADPG (h) and

UDPG (i) in WT, *BnaC02.TPS8* mutants (CR-44 and CR-153; WT, 'Westar') and overexpression lines (OE-33 and OE-38; WT, 'ZS11'). Data were obtained from the 5th and 6th leaves of seven-week-old seedlings grown hydroponically. Data are shown as the mean ± SD (n=6). Significant differences: *$P < 0.05$, **$P < 0.01$ and ns indicates not significant (Student's *t*-test).

Figure 4. Impact of *BnaC02.TPS8* on the concentration of glycolytic intermediates and organic acid in the leaves. (a-l) Concentrations of 3PGA (a), PEP (b), pyruvate (c), PEP: Pyruvate (d), shikimate (e), citrate (f), aconitate (g), isocitrate (h), 2-OG (i), succinate (j), fumarate (k) and malate (l) in WT, *BnaC02.TPS8* mutants (CR-44 and CR-153; WT, 'Westar'), and overexpression lines (OE-33 and OE-38; WT, 'ZS11'). Data were obtained from the 5th and 6th leaves of seven-week-old seedlings grown hydroponically. Data are shown as the mean ± SD (n=6). Significant differences: *$P < 0.05$, **$P < 0.01$ and ns indicates not significant (Student's *t*-test). 3PGA: 3-phosphoglycerate; PEP: phosphoenolpyruvate; 2-OG: 2-oxoglutarate.

Figure 5. Impact of *BnaC02.TPS8* on enzyme activities related to sucrose metabolism, starch synthesis, and trehalose-6-phosphate (TPS) activity in the leaves. (a-g) Enzyme activities including sucrose phosphate synthase (a), soluble acid invertase (b), neutral invertase (c), sucrose synthase (d), pyruvate kinase (e), AGPase (f), and TPS (g) in WT, *BnaC02.TPS8* mutants (CR-44 and CR-153; WT, 'Westar'), and overexpression lines (OE-33 and OE-38; WT, 'ZS11'). Data were obtained from the 5th and 6th leaves of seven-week-old seedlings grown hydroponically. Data are shown as the mean ± SD (n=6). Significant differences: *$P < 0.05$, **$P < 0.01$ (Student's *t*-test). AGPase: adenosine diphosphate-glucose pyrophosphorylase; TPS: trehalose-6-phosphate synthase.

Figure 6. Impact of *BnaC02.TPS8* on the expression of starch synthesis, starch degradation, and sugar metabolite transport-related genes in leaves, and nitrogen uptake and metabolism-related genes in roots. (a-l) Gene expression level of *GBSS1* (a), *SBE2.1* (b), *SBE2.2* (c), *GWD3*/*PWD* (d), *BAM1* (e), *BAM3* (f), *PPT* (g), *GLT1* (h), *SUC2* (i), *NRT1.1* (j), *NRT1.5* (k) and *GLN1* (l) in WT, *BnaC02.TPS8* mutants (CR-44 and CR-153; WT, 'Westar') and overexpression lines (OE-33 and OE-38; WT, 'ZS11').

The data in (a-i) and in (j-l) were collected from the 5th and 6th leaves of the plants, and roots of seven-week-old seedlings grown hydroponically, respectively. *BnaEF1-α* and *BnaActin2* were used as reference genes. Data are shown as the mean ± SD (n=4). Significant differences: **P* < 0.05, ***P* < 0.01 (Student's *t*-test). *GBSS1*, g*ranule-bound starch synthase1*; *SBE2.1*, *starch branching enzyme2.1*; *SBE2.2*, *starch branching enzyme2.2*; *GWD3/PWD*, *glucan water dikinase3*/ *phosphoglucan water dikinase*; *BAM1*, *β-amylase1*; *BAM3*, *β-amylase3*; *PPT*, *phosphoenolpyruvic acid translocater*; *GLT1*, *glucose-6-phosphate translocater*; *SUC2*, *sucrose transporter2*; *NRT1.1*, *nitrate transporter1.1*; *NRT1.5*, *nitrate transporter1.5*; *GLN1*, *glutamine synthetase1*.

Figure 7. Impact of *BnaC02.TPS8* on plant height and seed yield under high nitrogen (N) and low N conditions. (a) Phenotypic characterization of WT, *BnaC02.TPS8* mutants (CR-44 and CR-153; WT, Westar) and overexpression lines (OE-33 and OE-38; WT, ZS11) at the flowering stage under high N and low N conditions. (e-f) Plant height (e), and seed yield (f) of WT, *BnaC02.TPS8* mutants and overexpression lines under high N (180 kg N ha^{-1}) and low N (72 kg N ha^{-1}) conditions. Scale bars: 5 cm in (a-d). Data are shown as the mean ± SD (n=6 for (e) and n=4 for (f)). Different letters represent significant differences at *P* < 0.05, based on an ANOVA analysis with Tukey's significant difference test.

Figure 8. Impact of *BnaC02.TPS8* on the concentration of seed oil, protein, soluble sugar, and starch in mature seeds, the photosynthetic rate of pods, and the expression of starch synthesis and seed oil synthesis-related genes in developing seeds. (a-d) Seed oil (a), seed protein (b), seed soluble sugar (c), and seed starch (d) in the mature seeds of WT, *BnaC02.TPS8* mutants (CR-44 and CR-153; WT, Westar) and *BnaC02.TPS8* overexpression lines (OE-33 and OE-38; WT, ZS11). (e) Net photosynthetic rate of 40 DAF pods, (f-l) expression of genes related to starch synthesis: *GBSS1* (f) and *GBSS2* (g), fatty acid synthesis: *WRI1* (h), *MCAMT* (i), *FATA* (j), and oil storage: *OBO* (k) and *CALO* (l). RNA was extracted from 35 DAF seeds. *BnaEF1-α* and *BnaActin2* were used as reference genes. Data are shown as the mean ± SD (n=7 for (a-e); n=4 for (f-l)). Significant differences: **P* < 0.05, ***P* < 0.01 (Student's *t*-test). DAF, day after flowering. *GBSS1*, *granule-bound starch synthase1*; *GBSS2*, *granule-bound starch*

1125 *synthase1*; *WRI1*, *wrinkled1*; *MCAMT*, *malonyltransferase*; *FATA*, *acyl-ACP*
1126 *thioesterase A*; *OBO1*, *oil body oleosin1*; *CALO*, *caleosin*.

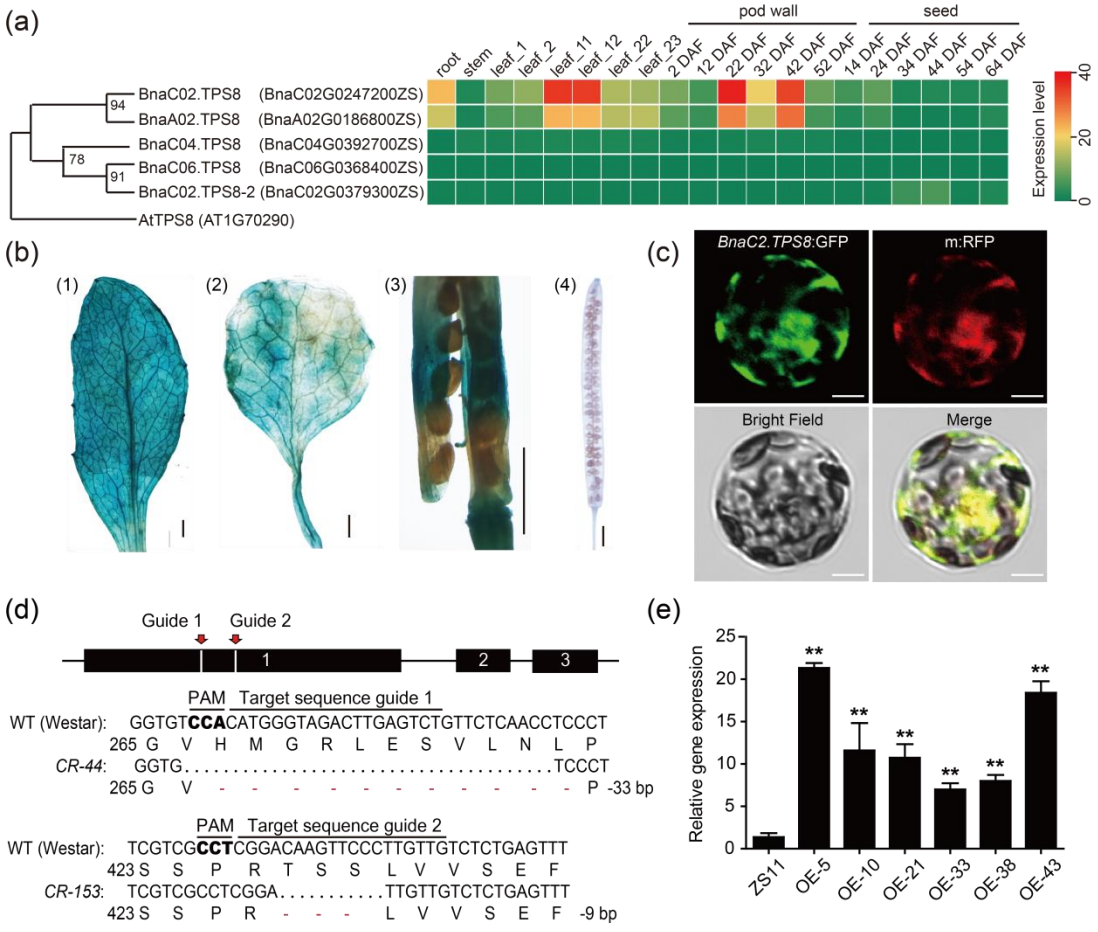

Figure 1. Gene expression pattern, protein localization, and generation of CRISPR/Cas9 mutants, and overexpression transgenic plants of *BnaC02.TPS8*. (a) Phylogenetic tree and gene expression pattern of *BnaC02.TPS8* in *B. napus*. Gene expression data were sourced from BnTIR (http://yanglab.hzau.edu.cn). At, *Arabidopsis thaliana*; Bn, *Brassica napus*. (b) Expression pattern of the *pBnaC02.TPS8* reporter gene in green stem leaf (1) and senescent rosette leaf (2) of post-flowering stage plants, and green silique (3) and yellow silique (4) of silique stage plants. Scale bars: 1 cm. (c) Subcellular localization of BnaC02.TPS8-GFP in *Arabidopsis* protoplast. GFP indicates the green fluorescent protein (GFP) fluorescence, while red indicates the cytosol marker fluorescence. Scale bars: 10 μm. (d) Mutagenesis of target sequence guided by 1 and 2 of the *BnaC02.TPS8* gene. (e) Relative gene expression of *BnaC02.TPS8* in *B. napus* shoots of wild type (cultivar 'ZS11') and *BnaC02.TPS8* overexpression (OE) lines. *BnaEF1-α* and *BnaActin2* were used as the references. Values are the means ± SD (n=4). Significant differences: $^{**}P < 0.01$ (Student's *t*-test).

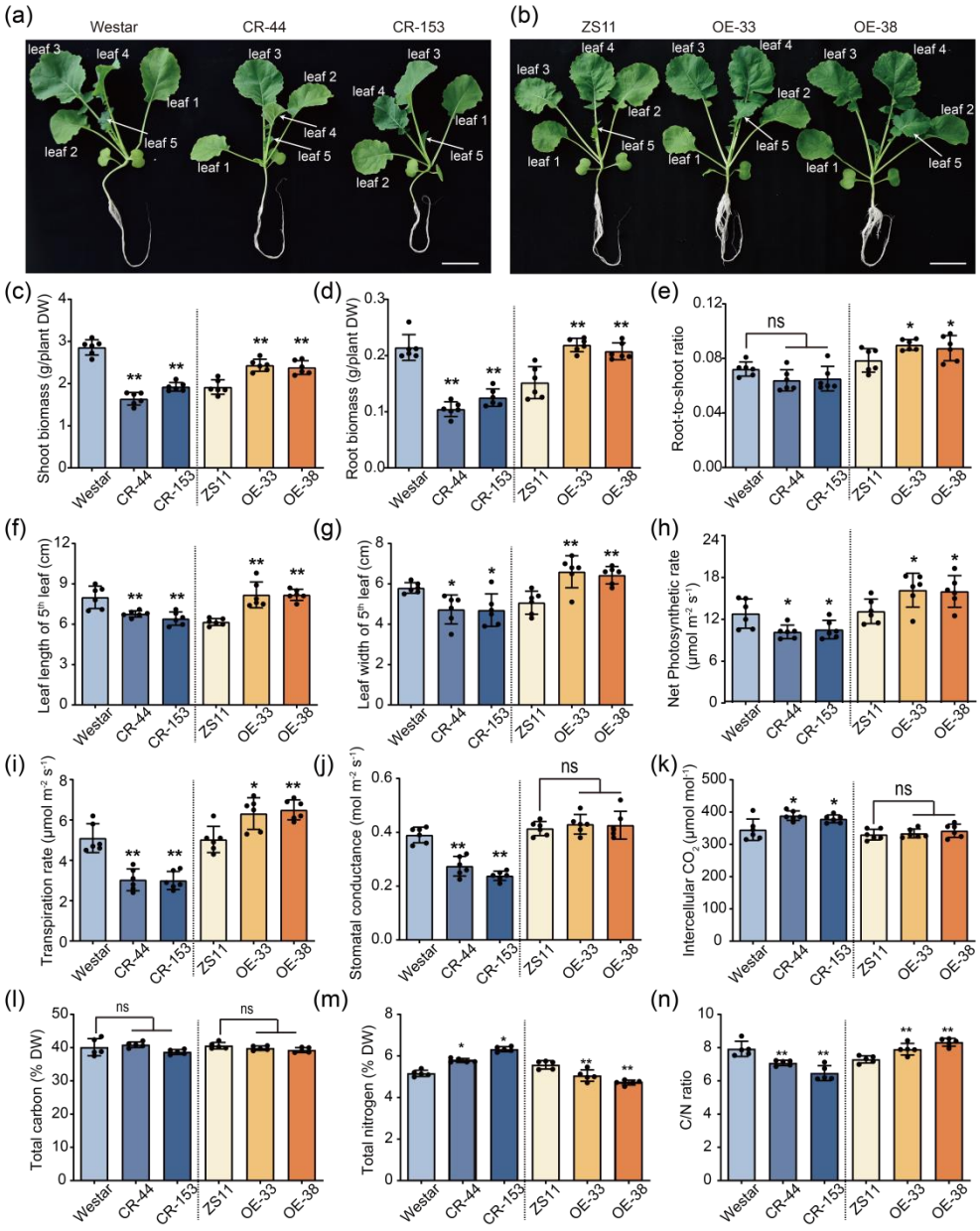

Figure 2. Impact of *BnaC02.TPS8* on the growth of *B. napus*. (a-b) Growth phenotype of five-week-old seedlings of CRISPR/Cas9 mutants (CR-44 and CR-153; WT, 'Westar') and overexpression lines (OE-33 and OE-38; WT, 'ZS11') grown hydroponically. Scale bars: 2 cm. (c-e) Shoot biomass (c), root biomass (d), and root-to-shoot ratio (e) of seven-week-old seedlings of WT, *BnaC02.TPS8* mutants and overexpression lines. (f-g) Leaf length (f) and leaf width (g) of the 5th leaf of the seven-week-old seedlings. (h-n) Net photosynthetic rate (h), transpiration rate (i), stomatal conductance (j), and intercellular CO_2 (k) measured in ten-week-old seedlings grown hydroponically. (l-n) Total carbon (l), total nitrogen (m), and C/N ratio (n) measured in the 5th and 6th leaves of the seven-week-old seedlings. The data in (c-n) are shown as the mean ± SD (n=6). Significant differences: *$P < 0.05$, **$P < 0.01$ and ns indicates not significant (Student's *t*-test).

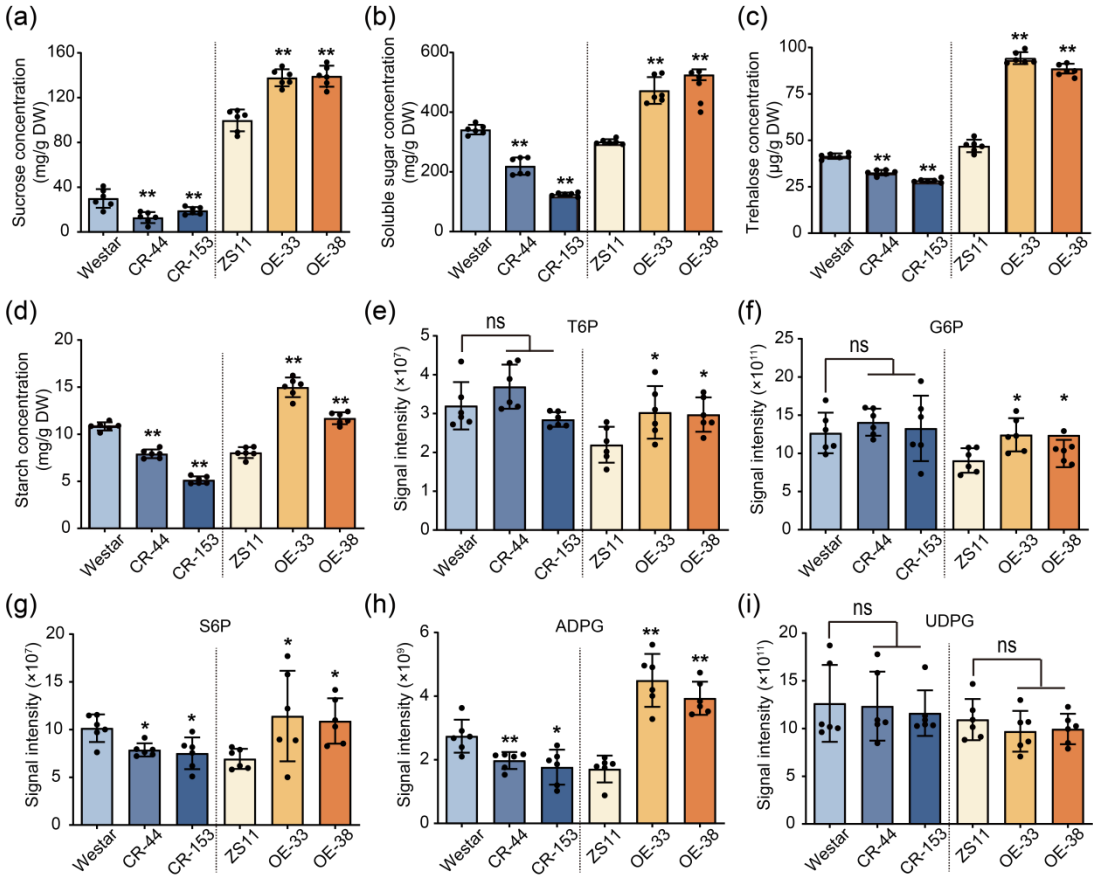

Figure 3. Impact of *BnaC02.TPS8* on the concentration of sugars, starch, sugar-phosphates, and sugar-nucleotides in the leaves. (a-i) Concentrations of sucrose (a), soluble sugar (b), trehalose (c), starch (d), T6P (e), G6P (f), S6P (g), ADPG (h) and UDPG (i) in WT, *BnaC02.TPS8* mutants (CR-44 and CR-153; WT, 'Westar') and overexpression lines (OE-33 and OE-38; WT, 'ZS11'). Data were obtained from the 5th and 6th leaves of seven-week-old seedlings grown hydroponically. Data are shown as the mean ± SD (n=6). Significant differences: *$P < 0.05$, **$P < 0.01$ and ns indicates not significant (Student's *t*-test).

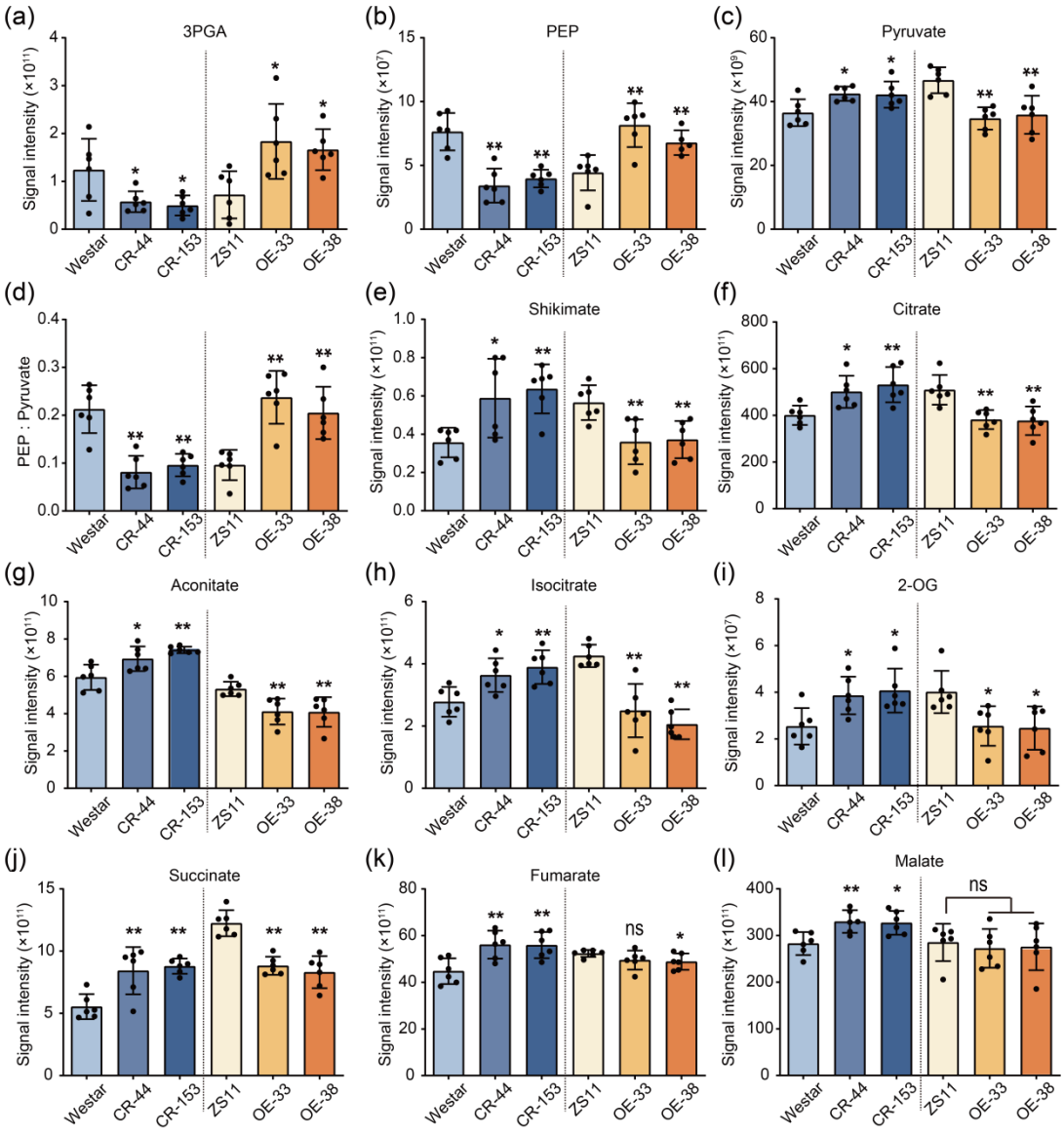

Figure 4. Impact of *BnaC02.TPS8* on the concentration of glycolytic intermediates and organic acid in the leaves. (a-l) Concentrations of 3PGA (a), PEP (b), pyruvate (c), PEP: Pyruvate (d), shikimate (e), citrate (f), aconitate (g), isocitrate (h), 2-OG (i), succinate (j), fumarate (k) and malate (l) in WT, *BnaC02.TPS8* mutants (CR-44 and CR-153; WT, 'Westar'), and overexpression lines (OE-33 and OE-38; WT, 'ZS11'). Data were obtained from the 5th and 6th leaves of seven-week-old seedlings grown hydroponically. Data are shown as the mean ± SD (n=6). Significant differences: *$P < 0.05$, **$P < 0.01$ and ns indicates not significant (Student's *t*-test). 3PGA: 3-phosphoglycerate; PEP: phosphoenolpyruvate; 2-OG: 2-oxoglutarate.

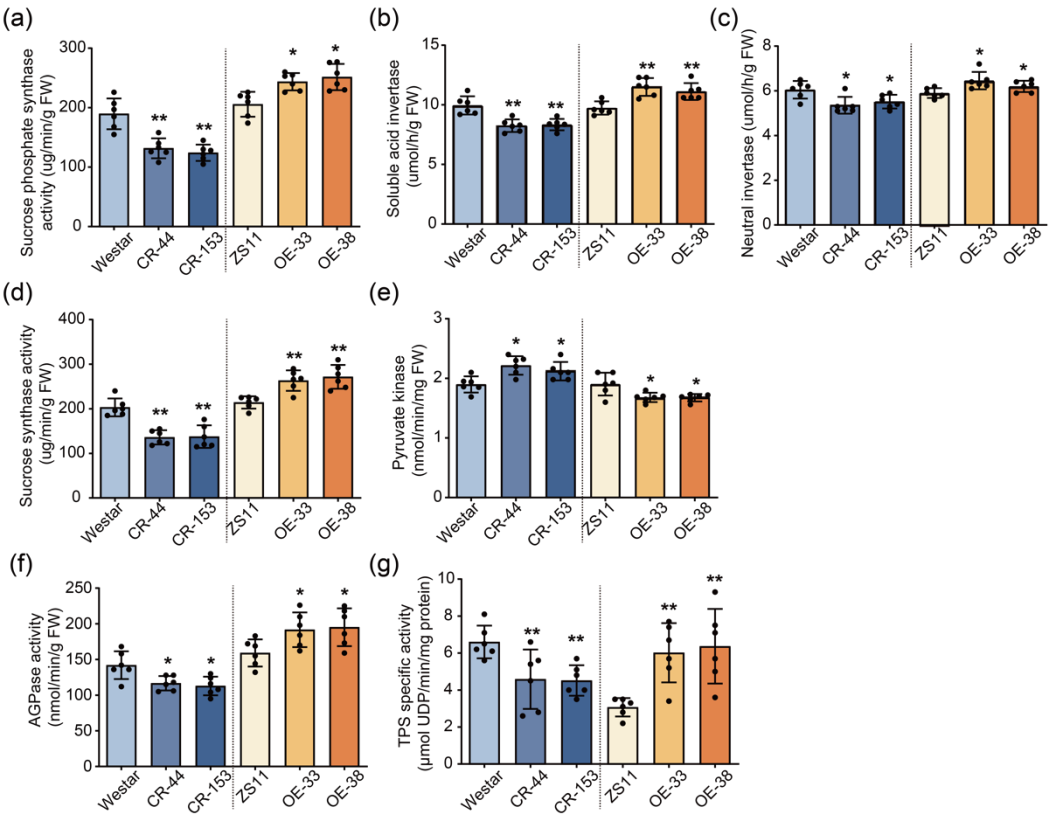

Figure 5. Impact of *BnaC02.TPS8* on enzyme activities related to sucrose metabolism, starch synthesis, and trehalose-6-phosphate (TPS) activity in the leaves. (a-g) Enzyme activities including sucrose phosphate synthase (a), soluble acid invertase (b), neutral invertase (c), sucrose synthase (d), pyruvate kinase (e), AGPase (f), and TPS (g) in WT, *BnaC02.TPS8* mutants (CR-44 and CR-153; WT, 'Westar'), and overexpression lines (OE-33 and OE-38; WT, 'ZS11'). Data were obtained from the 5th and 6th leaves of seven-week-old seedlings grown hydroponically. Data are shown as the mean ± SD (n=6). Significant differences: *P < 0.05, **P < 0.01 (Student's t-test). AGPase: adenosine diphosphate-glucose pyrophosphorylase; TPS: trehalose-6-phosphate synthase.

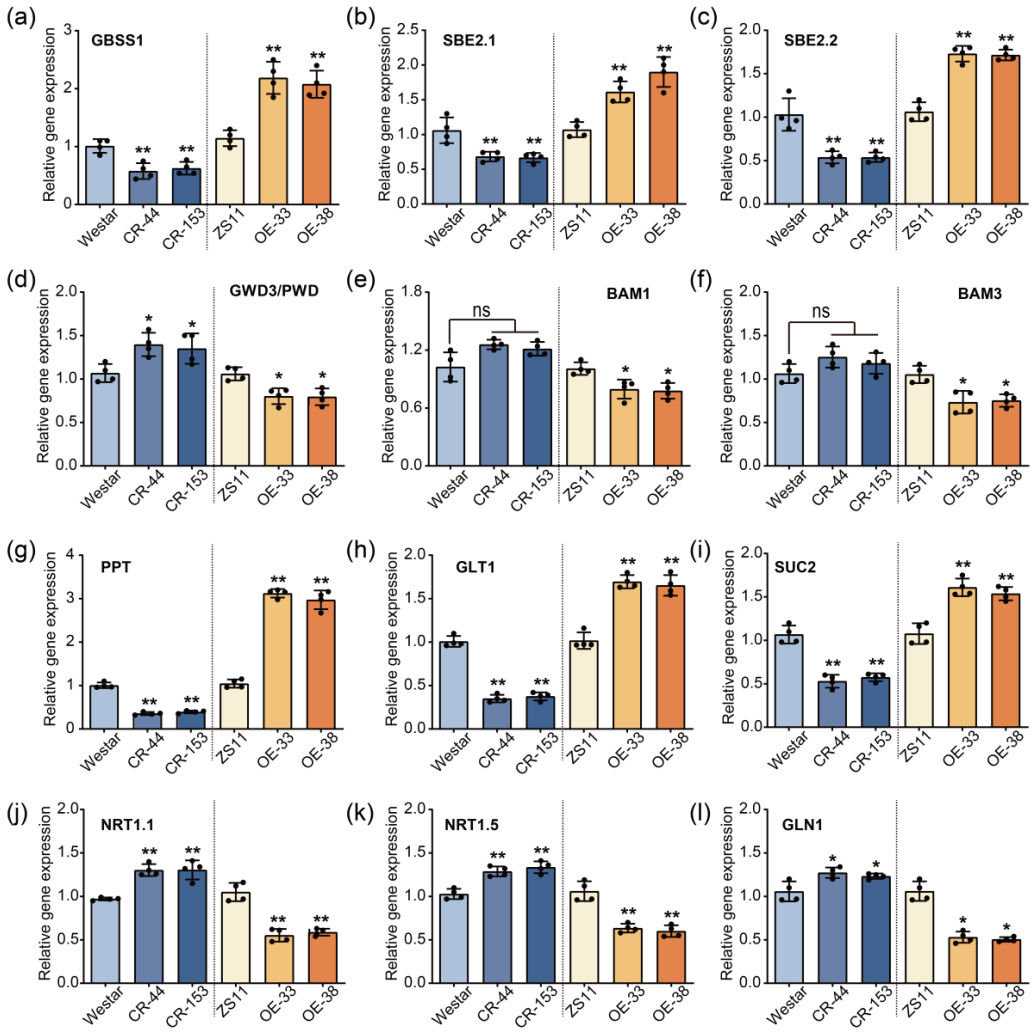

Figure 6. Impact of *BnaC02.TPS8* on the expression of starch synthesis, starch degradation, and sugar metabolite transport-related genes in leaves, and nitrogen uptake and metabolism-related genes in roots. (a-l) Gene expression level of *GBSS1* (a), *SBE2.1* (b), *SBE2.2* (c), *GWD3/PWD* (d), *BAM1* (e), *BAM3* (f), *PPT* (g), *GLT1* (h), *SUC2* (i), *NRT1.1* (j), *NRT1.5* (k) and *GLN1* (l) in WT, *BnaC02.TPS8* mutants (CR-44 and CR-153; WT, 'Westar') and overexpression lines (OE-33 and OE-38; WT, 'ZS11'). The data in (a-i) and in (j-l) were collected from the 5th and 6th leaves of the plants, and roots of seven-week-old seedlings grown hydroponically, respectively. *BnaEF1-α* and *BnaActin2* were used as reference genes. Data are shown as the mean ± SD (n=4). Significant differences: **P* < 0.05, ***P* < 0.01 (Student's *t*-test). *GBSS1*, *granule-bound starch synthase1*; *SBE2.1*, *starch branching enzyme2.1*; *SBE2.2*, *starch branching enzyme2.2*; *GWD3/PWD*, *glucan water dikinase3*/ *phosphoglucan water dikinase*; *BAM1*, *β-amylase1*; *BAM3*, *β-amylase3*; *PPT*, *phosphoenolpyruvic acid translocater*; *GLT1*, *glucose-6-phosphate translocater*; *SUC2*, *sucrose transporter2*; *NRT1.1*, *nitrate transporter1.1*; *NRT1.5*, *nitrate transporter1.5*; *GLN1*, *glutamine synthetase1*.

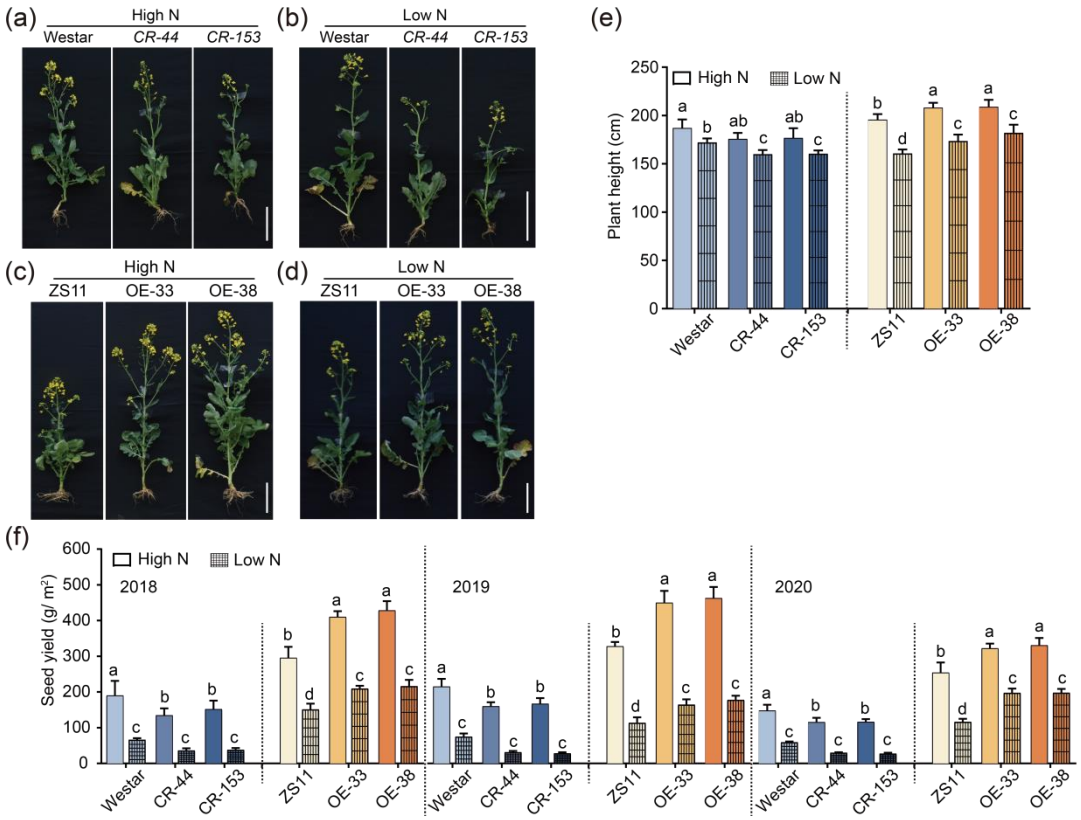

Figure 7. Impact of *BnaC02.TPS8* on plant height and seed yield under high nitrogen (N) and low N conditions. (a) Phenotypic characterization of WT, *BnaC02.TPS8* mutants (CR-44 and CR-153; WT, Westar), and overexpression lines (OE-33 and OE-38; WT, ZS11) at the flowering stage under high N and low N conditions. (e-f) Plant height (e), and seed yield (f) of WT, *BnaC02.TPS8* mutants, and overexpression lines under high N (180 kg N ha^{-1}) and low N (72 kg N ha^{-1}) conditions. Scale bars: 5 cm in (a-d). Data are shown as the mean ± SD (n=6 for (e) and n=4 for (f)). Different letters represent significant differences at $P < 0.05$, based on an ANOVA analysis with Tukey's significant difference test.

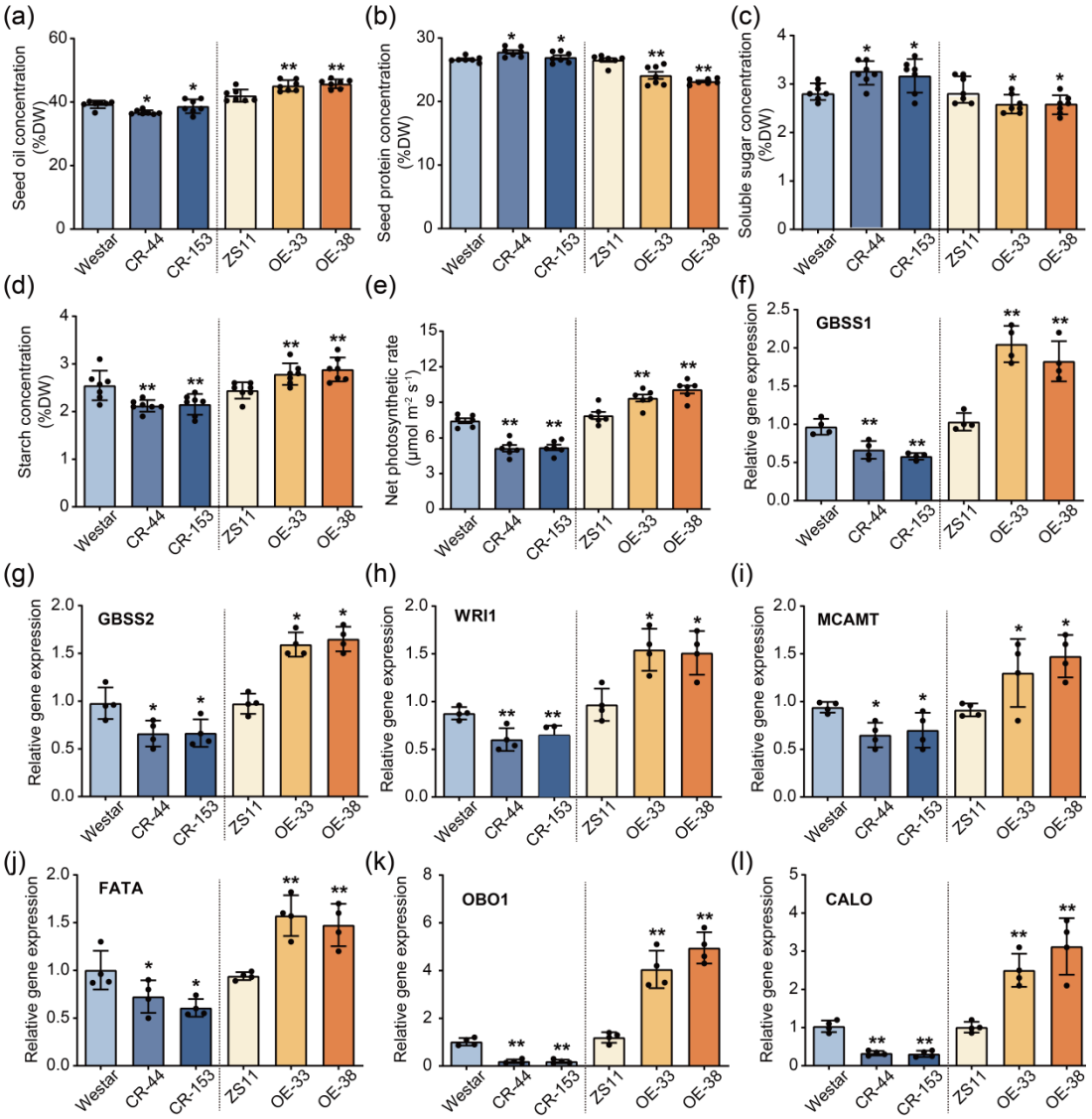

Figure 8. Impact of *BnaC02.TPS8* on the concentration of seed oil, protein, soluble sugar, and starch in mature seeds, the photosynthetic rate of pods, and the expression of starch synthesis and seed oil synthesis-related genes in developing seeds. (a-d) Seed oil (a), seed protein (b), seed soluble sugar (c), and seed starch (d) in the mature seeds of WT, *BnaC02.TPS8* mutants (CR-44 and CR-153; WT, Westar) and *BnaC02.TPS8* overexpression lines (OE-33 and OE-38; WT, ZS11). (e) Net photosynthetic rate of 40 DAF pods, (f-l) expression of genes related to starch synthesis: *GBSS1* (f) and *GBSS2* (g), fatty acid synthesis: *WRI1* (h), *MCAMT* (i), *FATA* (j), and oil storage: *OBO* (k) and *CALO* (l). RNA was extracted from 35 DAF seeds. *BnaEF1-α* and *BnaActin2* were used as reference genes. Data are shown as the mean ± SD (n=7 for (a-e); n=4 for (f-l)). Significant differences: $*P < 0.05$, $**P < 0.01$ (Student's *t*-test). DAF, day after flowering. *GBSS1*, *granule-bound starch synthase1*; *GBSS2*, *granule-bound starch synthase1*; *WRI1*, *wrinkled1*; *MCAMT*, *malonyltransferase*; *FATA*, *acyl-ACP thioesterase A*; *OBO1*, *oil body oleosin1*; *CALO*, *caleosin*.